

This discussion paper is/has been under review for the journal Atmospheric Chemistry and Physics (ACP). Please refer to the corresponding final paper in ACP if available.

Sensitivity of mesoscale model urban boundary layer meteorology to urban morphology

D. D. Flagg^{1,*} and P. A. Taylor¹

¹York University, Toronto, Ontario, Canada

*now at: Universität Hamburg, Hamburg, Germany

Received: 28 July 2010 – Accepted: 28 September 2010 – Published: 3 November 2010

Correspondence to: D. D. Flagg (ddflagg@yorku.ca)

Published by Copernicus Publications on behalf of the European Geosciences Union.

Sensitivity of mesoscale model urban boundary layer

D. D. Flagg and
P. A. Taylor

Title Page

Abstract

Introduction

Conclusions

References

Tables

Figures

⏪

⏩

◀

▶

Back

Close

Full Screen / Esc

Printer-friendly Version

Interactive Discussion

Abstract

Mesoscale modeling of the urban boundary layer requires careful parameterization of the surface due to its heterogeneous morphology. Model estimated meteorological quantities, including the surface energy budget and canopy layer variables, will respond accordingly to the scale of representation. This study examines the sensitivity of the surface energy balance, canopy layer and boundary layer meteorology to the scale of urban surface representation in a real urban area (Detroit-Windsor (USA-Canada)) during several dry, cloud-free summer periods. The model used is the Weather Research and Forecasting (WRF) model with its coupled single-layer urban canopy model. Some model verification is presented using measurements from the Border Air Quality and Meteorology Study (BAQS-Met) 2007 field campaign and additional sources. Case studies span from “neighborhood” (10 s ~ 30 m) to very coarse (120 s ~ 3.7 km) resolution. Small changes in scale can affect the classification of the surface, affecting both the local and grid-average meteorology. Results indicate high sensitivity in turbulent latent heat flux from the natural surface and sensible heat flux from the urban canopy. Small scale change is also shown to delay timing of a lake-breeze front passage and can affect the timing of local transition in static stability.

1 Introduction

The urban boundary layer (UBL) is a term frequently used to refer to the atmospheric boundary layer (ABL) over an urban area, a type of ABL distinguished by its underlying complex and heterogeneous surface. Analogous to a tall vegetation canopy, the urban surface consists of buildings that disrupt the flow of air within and above, generating turbulent eddies and reducing wind speed in the vicinity of the canopy (roof) top and within the canopy (Roth, 2000). In addition, the urban surface is typically composed of artificial materials (asphalt, concrete, brick, etc.) whose physical (e.g., albedo, thickness, evaporation efficiency) and thermodynamic properties (e.g., heat capacity, thermal conductivity, emissivity) often differ greatly from natural surfaces (Oke, 1987).

Sensitivity of mesoscale model urban boundary layer

D. D. Flagg and
P. A. Taylor

Title Page

Abstract

Introduction

Conclusions

References

Tables

Figures

⏪

⏩

◀

▶

Back

Close

Full Screen / Esc

Printer-friendly Version

Interactive Discussion



Consequently, these artificial surfaces and additional anthropogenic sources can alter the local energy balance. This combination of disruption to the local dynamics and energy balance has broad local and regional implications on meteorology and air quality.

The depth of the roughness sublayer (RSL) over vegetation typically varies from 0.5 to 50 m above the ground (Garratt, 1992) or approximately $2 \times z_R$ to $5 \times z_R$ or more (Roth, 2000), where z_R is the roughness element height. Where tall buildings are the roughness elements, the observed RSL depth may occupy the bulk of the surface layer (Rotach, 1999; Barlow and Coceal, 2009), substantially affecting the flow in and around the urban area. The urban RSL can be further subdivided into a shear layer, above the height of the local structure (canopy) rooftop, and a canyon layer below. In the shear layer, the logarithmic wind profile likely holds (Cheng and Castro, 2002). Within the canyon layer, however, the observed wind profile is often described as exponential (Macdonald, 2000), requiring alternate formulation. In addition, the urban RSL is particularly sensitive to the structural height (Cheng and Castro, 2002), orientation, dimension and density, collectively referred to as the urban “morphology”. The turbulent motions and circulations with and above the urban canopy affect the rate and direction of dispersion of pollutants within and above the urban canyon, contributing to the local air quality (Klein et al., 2007).

The urban surface energy budget is also sensitive to the morphology (Oke, 1981, 1982). Tall buildings can cast shadows, reducing the infiltration of direct short wave radiation into urban canyons, while potentially increasing diffuse radiation via reflection (Mills, 2004). Tall buildings can also reduce canyon wind speed, limiting the upward turbulent heat flux and canyon ventilation. These buildings can also act as heat storage mechanisms, increasing daytime up-take and nighttime emission to the urban environment. This effect may be considered part of an anthropogenic heat flux contribution to the energy budget (Nunez and Oke, 1977; Sailor, 2009), which can also include contributions from vehicular exhaust, industrial effluents and building ventilation. Another important part of the urban morphology is the presence of vegetated surfaces, which can contribute substantially to turbulent flux of latent heat.

Sensitivity of mesoscale model urban boundary layer

D. D. Flagg and
P. A. Taylor

[Title Page](#)[Abstract](#)[Introduction](#)[Conclusions](#)[References](#)[Tables](#)[Figures](#)[Back](#)[Close](#)[Full Screen / Esc](#)[Printer-friendly Version](#)[Interactive Discussion](#)

Sensitivity of mesoscale model urban boundary layer

D. D. Flagg and
P. A. Taylor

Title Page

Abstract

Introduction

Conclusions

References

Tables

Figures



Back

Close

Full Screen / Esc

Printer-friendly Version

Interactive Discussion



Early modeling work evaluated the UBL in one and two-dimensional simulations, treating the urban surface as a rough-wall, (a.k.a., “slab”, “sandbox” approach), (Myrup, 1969; Delage and Taylor, 1970; Vukovich, 1973; Bornstein, 1975). Current efforts to numerically model the UBL span a variety of approaches. Recent computational fluid dynamics (CFD) studies focus on simulating flow within the urban canyon or an idealized channel. Such CFD approaches include Direct Numerical Simulation (DNS): (Leonardi et al., 2003) Reynolds Averaged Navier-Stokes (RANS): (Kim and Baik, 1999) and Large-Eddy Simulation (LES): (Walton et al., 2002; Walton and Cheng, 2002). A viable compromise of computational efficiency and accuracy of dynamics and thermodynamics in the urban environment is the mesoscale NWP approach. Mesoscale models alone can only parameterize these processes in bulk subject to the scale of the surface land cover representation. Studies seeking to simulate the real urban environment through this approach often adopt an urban canopy model (UCM) or similar parameterizations (Masson, 2000; Kusaka et al., 2001; Martilli et al., 2002; Lee and Park, 2008; and Miao et al., 2009).

This study evaluates urban meteorology at the mesoscale using a coupled urban canopy model and numerical weather prediction (NWP) model. In balancing the computational cost of a large NWP model with the need for accuracy, of critical concern is the optimal scale for representation. There is a need to understand the nature of the error in the model meteorology that evolves from a reduced scale of surface representation. This study investigates the sensitivity of model estimated meteorology over a real urban area. Section 2 outlines the model and methods adopted. Section 3 offers model verification. Section 4 outlines the principal results and analysis and Sect. 5 offers conclusions.

2 Method

2.1 WRF-ARW model

This study uses the Weather Research and Forecasting Model (WRF) Advanced Research (ARW) version 2.2 (Skamarock et al., 2007) to simulate the mesoscale meteorology. The model time integration uses a third-order Runge-Kutta scheme; horizontal advection of momentum and scalars uses a fifth-order scheme, third-order in the vertical. This study makes use of the model's Rayleigh damping term to stabilize vertical momentum when the vertical velocity approaches the Courant number for stability as well as a sixth-order numerical diffusion term in the horizontal momentum equations to filter short-wave numerical noise. Horizontal eddy viscosity is determined from the Smagorinsky first-order closure method (Smagorinsky, 1963). Two-way interactive nested grids are invoked, with a 4-grid point relaxation zone boundary condition.

This study selects the Mellor-Yamada-Janjic (MYJ) ABL scheme (Janjic, 2002) and accompanying Eta surface layer model to parameterize the ABL. Vegetation and other land surface processes are parameterized using the Noah land surface model (LSM) (Chen and Dudhia, 2001). Cloud microphysics is parameterized according to the WRF Single Moment 3-Class scheme (Hong et al., 2004). Cumulus cloud parameterization is applied only in the coarsest model grid (see Sect. 2.2) according to the Kain-Fritsch scheme (Kain, 2004; Kain and Fritsch, 1993). Longwave radiation is parameterized according to Rapid Radiative Transfer Model of Mlawer et al. (1997) and shortwave radiation according to Chou and Suarez (1994). Initial conditions are taken from NCEP Eta 212 grid (40 km) model analysis (a.k.a., "AWIP") data available from the University Corporation for Atmospheric Research (UCAR) in three-hour increments at 26 vertical levels from 1000 hPa to 50 hPa. The AWIP data initializes the parent domain (see Sect. 2.2) and all nested grids at the start of model integration and provides boundary conditions for the parent domain.

Sensitivity of mesoscale model urban boundary layer

D. D. Flagg and
P. A. Taylor

Title Page

Abstract

Introduction

Conclusions

References

Tables

Figures



Back

Close

Full Screen / Esc

Printer-friendly Version

Interactive Discussion



Sensitivity of mesoscale model urban boundary layer

D. D. Flagg and
P. A. Taylor

Title Page

Abstract

Introduction

Conclusions

References

Tables

Figures

⏪

⏩

◀

▶

Back

Close

Full Screen / Esc

Printer-friendly Version

Interactive Discussion



To model the urban environment, WRF-ARW v2.2 provides a single layer urban canopy model (UCM) of Kusaka et al. (2001). This UCM represents urban areas as two-dimensional street canyons of infinite length without specified street orientation, designed as an extension to the Noah LSM. The UCM balances all energy sources locally at the four-layer road, wall and roof surfaces of each model grid cell: The surface energy balance is achieved independently at each surface (roof, wall and road) by iteratively (Newton-Raphson) manipulating the local skin surface temperature to adjust the heat fluxes the sum is sufficiently close to zero and the skin surface temperature (T_s) and diagnostic mean canyon air temperature (T_c) are in steady-state. The contribution of heat flux from each surface is scaled according to the normalized length of the roof (R), wall (h) and road (R_w) where $R + R_w = 1$. The LSM defines the (total) heat flux from the urban grid cell surface as the sum of flux from artificial/anthropogenic surfaces and the natural surface (grassland), partitioned according to the grid cell fractional coverage by the artificial surface (f_{URB}), e.g., for sensible heat flux:

$$H_{total} = f_{URB} H_{urban} + (1 - f_{URB}) H_{natural} \quad (1)$$

A diagnostic mean canyon wind speed is computed from an exponential function subject to the geometry of the canyon and speed of the flow above (Kusaka and Kimura, 2004). Further detail of the UCM and its coupling to WRF are presented by Kusaka et al. (2001) and Kusaka and Kimura (2004).

Some minor adjustments were made to the parameter settings for application to the Detroit-Windsor domain. The internal roof and wall temperature were set to 298.15 K to reflect a typical summertime interior building temperature. The internal road (ground) temperature was set to 295.25 K to reflect the approximate seasonal (JJA) average surface (2 m a.g.l.) temperature at Detroit-Windsor. A four-class urban land surface type approach (Grimmond and Oke, 1999) is used in place of the default three-class approach. Table 1 lists the principal gridded urban parameters by type, a blend of values recommended by Grimmond and Oke (1999) and morphological estimates from remote sensing imagery. The non-gridded urban parameters (e.g., surface albedo, thermal conductivity and surface emissivity, etc.) were selected following a review of

common parameterizations in the literature for similar implementations (Lee and Park, 2008; Miao et al., 2006; Kusaka and Kimura, 2004; Martilli, 2002 and Masson, 2000), in conjunction with default UCM values.

2.2 Domain

5 The area of interest is the Detroit-Windsor metropolitan area, estimated population: 4 726 779 (Statistics Canada, 2006, United States Census Bureau, 2010) straddling the USA-Canada border (Fig. 1). This urban area is located in the Great Lakes region of North America, an area of generally flat topography adjacent to multiple, large fresh water bodies. The Detroit River separates the cities of Detroit and Windsor and extends
10 from Lake St. Clair in the east to Lake Erie in the south. The model domain consists of one parent grid, stretching across the contiguous US and southern Canada, and three telescopically nested grids ($\Delta x = 37.5, 7.5, 1.5$ and 0.3 km, respectively). Grid 1 extends across 140 (86) gridpoints from west to east (north to south); both grids 2 and 3 are of squares of 36 gridpoints per side and grid 4 is a square of 66 gridpoints per
15 side. The model was run with 59 vertical levels and set to have approximately 21 levels in the lowest kilometer.

The resolution of the innermost grid (d04) approaches the limit of viability for application of the MYJ scheme to represent ABL turbulence; the scale of some eddies in the afternoon well-mixed layer in cases examined here likely briefly exceed the d04 grid scale. However, model TKE damping at the highest resolutions (energy cascade compensation) leads to an effective model resolution of approximately $7\Delta x$ (Skamarock, 2004), or approximately 2.1 km in d04 here. This scale exceeds h_{ABL} throughout the d04 grid in the test cases examined here. In addition, Miao et al. (2009) demonstrate
20 successful implementation of the MYJ ABL scheme in WRF at similarly high resolution (0.5 km) under fair-weather, warm-season conditions using the single layer UCM with comparable vertical resolution. Similarly, Guti errez et al. (2010) and Salamanca et al. (2010) indicate success with a 0.333 km grid scale using the Bougeault-Lacarr ere (BouLac) ABL scheme (Bougeault and Lacarr ere, 1989) with WRF, a TKE-prediction
25 scheme like MYJ.

Sensitivity of mesoscale model urban boundary layer

D. D. Flagg and
P. A. Taylor

Title Page

Abstract

Introduction

Conclusions

References

Tables

Figures



Back

Close

Full Screen / Esc

Printer-friendly Version

Interactive Discussion



the NOAA CRC dataset over Windsor. The resulting five blended, gridded land surface datasets are raster images of uniformly spaced pixels with categorical assignments to one of the 33 land surface types defined by the USGS NLCD (2001). Remote sensing imagery provided verification of the land surface raster images.

2.3 Case studies

The heterogeneity of the geometry, density and materials of the urban surface preclude explicit resolution of flow in a mesoscale model. The five gridded raster images of the Detroit-Windsor metropolitan area described above provide a source to understand how change in the representation of the urban surface under a common model resolution manifests through the model-estimated meteorology. This study runs five test cases, distinguished only by the scale of surface representation in arc-seconds (s): 10, 20, 30, 60 and 120.

The finest resolution case (10s) was chosen to reflect the “neighborhood” scale $O(10^2 \text{ m})$, capable of capturing the mean geometric and thermodynamic properties of a particular urban neighborhood without the need to explicitly resolve individual buildings or street canyons, as would likely be necessary at finer resolutions. Model estimates from case 10s runs represent the model’s best-guess for simulation of the meteorology. Departure from these model estimates in coarser case runs (20s, 30s...120s) represents sensitivity to the morphology of the urban environment, which varies with the scale of representation.

Analysis is mostly limited to the fourth model grid (Fig. 1), concentrating on two periods within the Border Air Quality and Meteorology Study (BAQS-Met) 2007 field campaign: 12:00 UTC 23 June–12:00 UTC 25 June 2007 (Period 1) and 00:00 UTC 7 July–00:00 UTC 8 July 2007 (Period 2), with the first six-hour period withheld from analysis to allow for model spin-up time. For both periods, local time in Detroit-Windsor is [UTC – 4] hours. The surface water temperature is held constant according to initial conditions throughout the duration of the model integrations. The two periods provide a useful archive for response under varying wind speed and direction. Both periods are

Sensitivity of mesoscale model urban boundary layer

D. D. Flagg and
P. A. Taylor

Title Page

Abstract

Introduction

Conclusions

References

Tables

Figures



Back

Close

Full Screen / Esc

Printer-friendly Version

Interactive Discussion



dry and generally cloud-free over the analysis area, dominated by synoptic-scale high pressure (1016–1019 hPa). In Period 1, nearly calm winds on 23 June yield to increasing south-southeast flow late on 24 June. Low-level winds gradually veer to southwest after 00:00 UTC 25 June as high and mid-level cloud cover increase gradually ahead of a weak extratropical cyclone. In Period 2, morning low-level wind speeds are nearly calm, increasing to 2–5 m s⁻¹ from the southwest by afternoon.

3 Model verification

To test the validity of model estimates in the urban boundary layer, a thorough verification of the model configuration is necessary. The BAQSMet 2007 field campaign included a series of flights by a Twin Otter aircraft measuring meteorological and chemical quantities at various heights across southwestern Ontario and adjacent areas around Detroit. The Twin Otter datasets serve as the crux of model verification data in the Detroit-Windsor domain, supported with additional data from radiosondes, METAR and a VHF wind profiler.

To complement this verification with a more precise diagnosis of model performance within and above the urban canopy, additional model comparison studies were conducted over Oklahoma City, OK, USA (omitted here). These comparison studies utilized measurements from the Joint Urban 2003 field campaign (Allwine et al., 2004) to verify model estimates.

3.1 Instrumentation

BAQS-Met 2007 field data includes a series of measurements taken on-board the National Research Council (NRC) Twin Otter Atmospheric Research Aircraft (hereinafter: Twin Otter). Instrumentation aboard included an array of air sampling equipment and meteorological instruments (Srinivasan and Bastian, 2008). Two flights crossed the urban core grid of the domain and are used here for model verification: Flight #12

Sensitivity of mesoscale model urban boundary layer

D. D. Flagg and
P. A. Taylor

Title Page

Abstract

Introduction

Conclusions

References

Tables

Figures



Back

Close

Full Screen / Esc

Printer-friendly Version

Interactive Discussion



(3–4 July 2007) and Flight #13 (6–7 July 2007). Measurements of three-dimensional wind, temperature (T), dew point temperature (T_d) and air pressure (p) were extracted for model verification.

Several additional stationary sources supplement Twin Otter data toward model verification. Radiosonde launches (with GPS) by the US National Weather Service (NWS) at White Lake, Michigan, (KDTX: 42.70° N, 83.47° W) provide a useful comparison for temperature, water vapor mixing ratio (q), wind speed (u) and wind direction (u_θ). This station is located within the second grid of the model domain, west of Detroit-Windsor. Profiles are extracted from the launch times nearest to Flights #12 and #13. During Twin Otter Flight #13, three missed landings took place at airports with hourly Aviation Routine Weather Reports (METAR) available from in-situ instruments at field level (Plymouth State University, 2010), two of which coincide within several minutes of METAR data, providing points of surface verification.

A VHF wind profiler installation at Harrow, ON (42°42' N 83°28' W), part of the Ontario-Quebec VHF Wind Profiler Network (Hocking and Hocking, 2007), provides hourly horizontal wind speed and direction measurements in 500 m range gates throughout much of the troposphere. Data is available for comparison during both study periods when and where sufficient signal return is present, but no data is available during Flight #12. The wind profiler is situated in the second model grid, approximately 50 km south-southeast of the urban core of Detroit-Windsor (Fig. 2).

3.2 Data quality control

Measurement of the true air velocity on-board the Twin Otter is subject to uncertainty caused by the blending of instrumentation to produce the final dataset (Srinivasan and Bastian, 2008). A correction was made to compensate for a systematic horizontal wind error for the two flights examined here (Ms. Katherine Hayden, Environment Canada, personal communication, 2009). To reduce bias in vertical velocity measurements, the 1 Hz instantaneous moments of vertical velocity were detrended by removing the mean vertical velocity.

Sensitivity of mesoscale model urban boundary layer

D. D. Flagg and
P. A. Taylor

Title Page

Abstract

Introduction

Conclusions

References

Tables

Figures

⏪

⏩

◀

▶

Back

Close

Full Screen / Esc

Printer-friendly Version

Interactive Discussion



Sensitivity of mesoscale model urban boundary layer

D. D. Flagg and
P. A. Taylor

Title Page

Abstract

Introduction

Conclusions

References

Tables

Figures

⏪

⏩

◀

▶

Back

Close

Full Screen / Esc

Printer-friendly Version

Interactive Discussion



To mitigate white noise in these datasets of 1 Hz sampling frequency, a one-minute average was taken for all variables. This averaging period was selected to facilitate model-measurement comparison; model estimates were archived in one-minute sampling intervals (instantaneous) for the duration of each flight. The 1 Hz data was retained for the calculation of turbulence kinetic energy (TKE) per unit mass.

To verify model estimates, this study uses a 16-point linear interpolation algorithm to map model estimates to observation space (Eq. 2). Given an observed variable y at $y(i_0, j_0, k_0, l_0)$ where i_0 and j_0 reflect the horizontal position, k_0 the vertical position and l_0 the temporal position, the algorithm seeks the nearest model estimates of the model variable x , which may be a variable identical to y or in need of conversion (e.g., dew point temperature to mixing ratio). The algorithm extracts x at the four model grid points surrounding $y(i_0, j_0, k_0, l_0)$ in horizontal, two-dimensional space at the two model vertical levels that enclose the height of the observation (k_0). The algorithm then extracts these eight points at the two model output times that enclose the observation time (l_0). The algorithm then interpolates the model variable to the point of observation, $\hat{x}(i_0, j_0, k_0, l_0)$, by applying weights to x at the 16 grid points determined earlier. The weights are inversely proportional to the three-dimensional distance (d) or time (t) between the model grid point and the observation according to Eq. (2)

$$\hat{x}(i_0, j_0, k_0, l_0) = \sum_{m=1}^2 \left(\frac{\frac{1}{t_m}}{\sum_{m=1}^2 \frac{1}{t_m}} \right) \sum_{n=1}^8 x_n(i_n, j_n, k_n, l_n) \cdot \left(\frac{\frac{1}{d_n}}{\sum_{n=1}^8 \frac{1}{d_n}} \right) \quad (2)$$

3.3 Flight #12

BAQS-Met 2007 Twin Otter Flight #12 crossed through the third grid of the model domain between 00:05 and 00:48 UTC 4 July 007, exiting the northwest corner of the domain for 15 minutes within that period for a course change at Oakland International Airport (KTPK) in Pontiac, Michigan, USA (Fig. 2a). Within the third model grid, the

flight level varies between roughly 300 to 500 m a.g.l., except in the final minutes when the aircraft descends to approximately 170 m a.g.l.

A majority of measurements are clustered near 510 m a.g.l. (Fig. 3). Comparison indicates a cold model bias in air temperature (Table 2), though this bias is noticeably smaller where Twin Otter data is most abundant. Mamrosh et al. (2002) report a mean bias of around +1 K for commercial aircraft (ACARS) measurements vs. adjacent radiosonde measurements (within 10 km), below 400 hPa. Ballish and Kumar (2008) find a bias of +0.6 to 1.5 K at 925 hPa using AMDAR data, which is roughly 20 to 40 hPa above most flight measurements here. Although instrumentation differs among these comparisons, this may partly explain the cold model bias. Comparing against 00Z 4 July 2007 radiosonde data (Fig. 4), model estimates overestimate temperature by 1–2 K in the lowest 2 km, and by ~2 K above that.

There is also a significant dry model bias (around -2.5 g kg^{-1}) relative to Twin Otter measurements (Table 2) that appears to be insensitive to height. This dry bias is not present in model comparison to the radiosonde data. Mamrosh et al. (2002) indicate a mean dew point temperature bias of approximately +1.8 K in ACARS data, offering one possible explanation.

Model performance with wind estimation is less clear; the model consistently overestimates scalar-average horizontal wind speed vs. Twin Otter measurements. Comparison with radiosonde data suggests model overestimation below the model-estimated boundary layer depth ($h_{\text{ABL}} \sim 939 \text{ m}$), with varying performance above. Wind direction also shows discrepancy vs. Twin Otter measurements. Some of this can be explained by the relatively light wind speeds. This discrepancy, together with an unexplained backing of the winds, leaves some uncertainty in the Twin Otter wind measurements. Model estimated wind direction shows strong coherence with the 00Z 4 July 2007 radiosonde data (Fig. 4), with a model RMSE of 7.79° for the full profile (Table 2). Model estimated TKE shows fairly strong coherence with observations, including a local peak near 400 m a.g.l. (not shown).

Sensitivity of mesoscale model urban boundary layer

D. D. Flagg and
P. A. Taylor

Title Page

Abstract

Introduction

Conclusions

References

Tables

Figures

⏪

⏩

◀

▶

Back

Close

Full Screen / Esc

Printer-friendly Version

Interactive Discussion



Sensitivity of mesoscale model urban boundary layer

D. D. Flagg and
P. A. Taylor

Title Page

Abstract

Introduction

Conclusions

References

Tables

Figures

⏪

⏩

◀

▶

Back

Close

Full Screen / Esc

Printer-friendly Version

Interactive Discussion



Examining model performance vs. time (Fig. 5), Twin Otter temperature measurements during an ascent near 00:12 UTC 4 July suggest a highly unstable local lapse rate of 13 K km^{-1} , not captured by the model. This observed feature is not replicated during the subsequent descent (00:37–00:48 UTC), whereas the model response is proportionally opposite. Similar behavior is shown for wind speed with Twin Otter measurements indicating steadily increasing wind speed during ascent. The horizontal wind speed shows the strongest coherence of model and measurement directly over downtown Detroit, at 510 m a.g.l. Comparison of wind speed to 00:00 UTC METAR at Windsor Airport (CYQG: 42.27° N , 82.97° W) reveals surface (10 m a.g.l.) winds of less than 2.5 m s^{-1} , justifying the Twin Otter measurements. For wind direction, Twin Otter measurements suggest erratic change over short distances and largely differ from METAR at CYQG (south at 00:00 UTC, south-southwest at 01:00 UTC) and Coleman A. Young International Airport (KDET: 42.42° N , 83.02° W , south-southeast at both 00:00 and 01:00 UTC). These METAR wind directions match very well with model estimated wind direction.

3.4 Flight #13

BAQS-Met 2007 Twin Otter Flight #13 crossed the third grid of the model domain between 10:03 and 10:57 UTC 7 July 2007, exiting the northwest corner of the domain for 13 min near the middle for a course change at KPTK (Fig. 2b). Within the third model grid, the flight level varies across the lowest 520 m a.g.l., including three missed landings at airports within the model grid (10:10, 10:21, 10:50 UTC). Being an early morning transect, measurement points fall above the model estimated h_{ABL} ($<200 \text{ m a.g.l.}$ throughout the period) except for the missed landings.

The vertical comparison (Fig. 3) confirms the cold and dry model bias seen in Flight #12, though both indicate a strong low-level temperature inversion. A model warm bias aloft vs. radiosonde data is apparent. However, the radiosonde may drift horizontally up to 300 km during a typical two-hour ascent (NOAA National Weather Service, 2010).

A model dry bias vs. Twin Otter measurements is present, as in Flight #12. Whereas model estimates suggest a generally uniform water vapor mixing ratio, Twin Otter

**Sensitivity of
mesoscale model
urban boundary layer**D. D. Flagg and
P. A. Taylor

Title Page

Abstract

Introduction

Conclusions

References

Tables

Figures

⏪

⏩

◀

▶

Back

Close

Full Screen / Esc

Printer-friendly Version

Interactive Discussion

measurements indicate significant fluctuation, varying by as much as 6 g kg^{-1} in the lowest 500 m a.g.l. (Fig. 3). This observed variation cannot be wholly explained by the flight path over Lake St. Clair, sudden wind shifts or any recent rainfall. There is a much stronger coherence of model estimates to radiosonde water vapor mixing ratio measurements, with RMSE under 1 g kg^{-1} and smaller mean bias. During the course of radiosonde ascent, model estimated h_{ABL} increases from 250 to 350 m a.g.l., suggesting that the model overestimation of mixing ratio may be sensitive to the h_{ABL} estimate (Fig. 4). Turner et al. (2003) report a dry bias of approximately 5% in their studies using the Vaisala RS80-H radiosonde (commonly used by NWS) with a general 5–10% difference in relative humidity measurements from a dual-launch of radiosondes. Miller et al. (1999) report a systematic dry bias in radiosonde measurements of relative humidity in comparison to both surface stations and aircraft measurements in the mixed layer. Thus, the model moist bias may be partly explained by a potential radiosonde measurement error.

The model overestimates scalar-average horizontal wind speed comparing against both Twin Otter and radiosonde measurements (Figs. 3 and 4), with an RMSE of $2\text{--}3 \text{ m s}^{-1}$. Comparison vs. the Harrow VHF wind profiler for 7 July, with a relative abundance of model-measurement comparison points, yields a similar RMSE but with an improved mean bias that suggests a slight model underestimation (Fig. 6). Thus, bias in the model estimation of horizontal wind speed remains uncertain, but at least some local overestimation is likely present. Limited surface measurements from the Twin Otter missed landings also support model overestimation (Table 3).

Model RMSE of wind direction vs. radiosonde and wind profiler measurements shows much less variability than that of Twin Otter measurements. Model estimates reasonably capture the profile of wind direction vs. Harrow measurements (Fig. 6) for both 7 July (Period 2) and Period 1. At both missed landings shown in Table 3, model estimated wind direction and METAR wind match very well, while Twin Otter measurements show noticeable departure.

Evaluating the model performance vs. time (Fig. 5), both missed landings at KDET show a pronounced spike in Twin Otter measured temperature not captured in the model. This may be due to interpolation of near surface temperature from local skin surface temperature and lowest vertical layer air temperature, potentially missing microscale variation. Though limited in number, model estimates are closer to METAR temperature than are the Twin Otter measurements (Table 3). The Twin Otter measures a sharp spike in mixing ratio at the CYQG missed landing (10:10 UTC), but not at either KDET missed landing, (10:21, 10:50 UTC) and shows a substantial increase in water vapor mixing ratio to the northwest, all absent from the model estimates. Model performance of mixing ratio is strong vs. METAR measurements at both the 10:10 and 10:50 missed landings (Table 3).

Model-estimated horizontal wind speed shows overestimation in time vs. Twin Otter measurements except over the urban core of Detroit (roughly 10:14–10:17 UTC) near 520 m.a.g.l. Twin Otter observations capture the wind speed decrease (increase) on the approach (take-off) of the missed landings more clearly than do model estimates. During the Flight #13 period, model-estimated and wind profiler-measured horizontal wind speed show strong coherence over the column (Fig. 6). Model performance of wind direction vs. Twin Otter observations is erratic in time (Fig. 5), with smallest bias at the time of missed landings.

3.5 Summary of model verification

Comparison of model temperature estimates with Twin Otter flight measurements yields a distinct model cold bias of 2–3 K over approximately the lowest 500 m.a.g.l. This bias may be influenced by a 1 K warm bias common to commercial aircraft temperature measurements. Conversely, model comparison to radiosonde measurements at KDTX reveals a warm bias of about 1 K in the corresponding vertical region and aloft with an RMSE of 2–4 K.

Twin Otter measurements of mixing ratio are consistently and significantly higher than both model estimates and METAR observations where overlap exists. The latter

Sensitivity of mesoscale model urban boundary layer

D. D. Flagg and
P. A. Taylor

Title Page

Abstract

Introduction

Conclusions

References

Tables

Figures



Back

Close

Full Screen / Esc

Printer-friendly Version

Interactive Discussion



2 sample F-test) between all cases for the f_{URB} parameter, but only compared with case 60 s and 120 s for z_R and R/R_W . These results establish a need to diagnose the response of the local meteorology to this statistically significant change in the urban morphology.

5 4.2 Quantifying the meteorological response

Analysis of the change in model meteorology over the urban core of Detroit-Windsor concentrates on two areas: the surface energy balance and the meteorology within and above the urban canopy, including static and dynamic stability, temperature, moisture, turbulence kinetic energy, horizontal and vertical winds and estimated boundary layer depth. The evaluation examines (1) change to the grid-average value of pertinent quantities, (2) sources of local change within the grid and (3) variation in time of the root-mean-squared-deviation (RMSD) of pertinent quantities between case studies. The latter assessment provides a sound estimate of the magnitude of change that can be anticipated as a result of using coarser mesoscale urban representation, effectively contributing a rough “error bar” to quantities of interest to mesoscale atmospheric modelers. The RMSD assessment includes comparisons of all case studies (10 s, 20 s, 30 s, 60 s, 120 s). The remaining assessments focus exclusively on the change from case 10 s to case 20 s to understand the significance of the neighborhood scale on urban meteorology and the magnitude of change resulting from a very small reduction in the scale of urban representation.

The change in land cover resolution from case 10 s to case 20 s creates an abundance of model grid cells with changed urban land cover type (Fig. 7). With the presence of the Detroit River, this also includes the transition of cells from urban to non-urban (including water) classification and vice versa. For grid-average values, a principal consequence of this change in land cover resolution is a slight shift in the overall distribution of urban land cover type toward higher urban intensities, masking some of the heterogeneity of the true urban surface.

Sensitivity of mesoscale model urban boundary layer

D. D. Flagg and
P. A. Taylor

Title Page

Abstract

Introduction

Conclusions

References

Tables

Figures



Back

Close

Full Screen / Esc

Printer-friendly Version

Interactive Discussion



4.3 Surface energy budget response

The surface energy budget for case 10s (Fig. 8) illustrates the contribution of both the urban and natural surfaces to the local energy balance. A shift in grid-average urban intensity from case 10s to case 20s perturbs this surface energy balance. The daytime skin surface temperature of the urban solid surfaces (roof, wall, road) peaks around 10 K higher than the natural surface in this study, preceding peak air temperature above the canopy (~22:00 UTC) by about 4 h (not shown). Consequently, this shift increases the grid-average skin surface temperature by up to 0.2 K (for a grid-average f_{URB} increase of 0.014). This result confirms expectations of increased surface (skin) temperature associated with increased urban intensity. The natural skin surface temperature incurs little change except where grid cells are reassigned from land to water cover or vice-versa as a result of resolution of the Detroit River.

For the urban canopy, the immediate effect of a shift toward higher grid-average urban intensity is geometric: a taller canopy with increased building density, restricting canyon space. This reduces u_c , enhancing the bulk transfer (drag) coefficient for heat (C_H) at the wall and road surfaces (C_H also increases at the roof). The net result favors enhanced sensible and latent flux from the urban canopy ($I_v E_{\text{urban}}$, H_{urban}). To restore equilibrium in the surface energy budget, the model iteratively reduces the skin surface temperature at the wall, road and roof surfaces, reducing G_{urban} , H_{urban} , $I_v E_{\text{urban}}$ and the outgoing (longwave) radiation. These urban fluxes are additionally sensitive to local temperature and moisture gradients.

Among all surface energy budget components, the latent heat flux ($I_v E_{\text{total}}$) demonstrates the most significant response between case 10s and case 20s (Fig. 9). The contribution from the urban component ($I_v E_{\text{urban}} f_{\text{URB}}$) is minimal due to limited moisture availability (β), remaining below 10 Wm^{-2} at peak. Thus, the change in $I_v E_{\text{total}}$ derives principally from the natural surface component of the grid cells, $(1 - f_{\text{URB}}) I_v E_{\text{natural}}$, during the daytime when $I_v E_{\text{natural}}$ is strongest. The change in f_{URB} contributes toward the bulk of the daytime decrease in $I_v E_{\text{total}}$ with $I_v E_{\text{natural}}$ responsible for the remainder. The latent heat flux from a vegetation-covered surface here derives mostly from canopy

Sensitivity of mesoscale model urban boundary layer

D. D. Flagg and
P. A. Taylor

Title Page

Abstract

Introduction

Conclusions

References

Tables

Figures

⏪

⏩

◀

▶

Back

Close

Full Screen / Esc

Printer-friendly Version

Interactive Discussion



Sensitivity of mesoscale model urban boundary layer

D. D. Flagg and
P. A. Taylor

Title Page

Abstract

Introduction

Conclusions

References

Tables

Figures

⏪

⏩

◀

▶

Back

Close

Full Screen / Esc

Printer-friendly Version

Interactive Discussion

evapotranspiration, parameterized by the Penman-Monteith relation (Monteith, 1981). The grid-average contributions to available energy changes little between cases; the change in $I_{\nu}E_{\text{natural}}$ derives largely from the water vapor demand at the lowest model layer (~ 28 m a.g.l.), which varies locally. The RMSD of $I_{\nu}E_{\text{total}}$ (Fig. 10) over the urban core peaks at 45 Wm^{-2} at 18:00 UTC (14:00 LT), coincident with the time of the strongest flux (Fig. 8) and nearly 25% of its value. RMSD increases monotonically, in phase, for case 10s vs. progressively coarser cases, approaching 35% of the total flux value for case 10s vs. case 120s. This demonstrates significant daytime sensitivity of model estimated $I_{\nu}E_{\text{total}}$ to the scale of urban representation and the potential gain from use of the neighborhood scale (case 10s) in urban surface representation. It also suggests that much coarser representations yield only a marginal increase in RMSD from the neighborhood scale.

The response of the surface sensible heat flux (H_{total}) to the land cover resolution change entails contributions from both the urban (H_{urban}) and natural (H_{natural}) surface components. Daytime grid-average H_{total} increases from case 10s to case 20s, the sum of an increase from $H_{\text{urban}}f_{\text{URB}}$ and a decrease from $H_{\text{natural}}(1-f_{\text{URB}})$ (Fig. 9). The net increase in f_{URB} reduces the proportion of total flux from natural surfaces contributing partly toward the early afternoon reduction of $H_{\text{natural}}(1-f_{\text{URB}})$. H_{natural} itself also decreases due to the reduced daytime natural surface skin temperature, shrinking the local natural skin surface-to-2 m temperature gradient and, hence, the flux.

While the grid-average contribution of $H_{\text{urban}}f_{\text{URB}}$ to H_{total} is positive, grid-average change to H_{urban} itself is negative. The skin surface temperature reduction along the canopy roof, walls and road grows to 0.5 K by mid-afternoon, with diagnostic canyon air temperature (T_c) decreasing by approximately half that. Additionally, the shift toward higher urban intensity favors greater building density, at the expense of canyon width. In the afternoons, the peak temperature difference between the roof surface and the air above the canopy ($\sim +6$ K) is considerably smaller than that between the canyon wall or road surfaces and the canyon air temperature ($\sim +9$ K, $+12$ K, respectively), not shown here. Combined, these changes reduce grid-average H_{urban} by approximately

Sensitivity of mesoscale model urban boundary layer

D. D. Flagg and
P. A. Taylor

Title Page

Abstract

Introduction

Conclusions

References

Tables

Figures

⏪

⏩

◀

▶

Back

Close

Full Screen / Esc

Printer-friendly Version

Interactive Discussion

8 Wm^{-2} by mid-afternoon from case 10 s to case 20 s. Despite the grid-average reduction of H_{urban} the grid-average increase of f_{URB} forces a net increase in grid-average $H_{\text{urban}}f_{\text{URB}}$. Accounting for those grid cells that change from urban to non-urban classification and vice versa (such as by consequence of resolution of the Detroit River), this further increases $H_{\text{urban}}f_{\text{URB}}$, resulting in a net increase of approximately 10 Wm^{-2} in mid-afternoon, a 4% enhancement of its original contribution in case 10 s (Fig. 8).

The RMSD of H_{total} (Fig. 10) over the urban core peaks at 62 Wm^{-2} around 17:30 UTC (13:30 LT), coincident with the time of the strongest $H_{\text{urban}}f_{\text{URB}}$ (Fig. 8) and 18% of H_{total} . As with $I_{\text{V}}E_{\text{total}}$, RMSD increases monotonically, in phase, for case 10 s vs. progressively coarser cases, approaching 27% of the total flux value for case 10 s vs. case 120 s, further demonstrating significant local sensitivity.

Grid-average change to ground heat flux (G_{total}) from case 10 s to 20 s is virtually negligible (Fig. 9), but is the result of opposing change in the urban ($G_{\text{urban}}f_{\text{URB}}$) and natural surface contributions $G_{\text{natural}}(1 - f_{\text{URB}})$ that can result in more substantial changes locally. The $G_{\text{natural}}(1 - f_{\text{URB}})$ contribution registers a grid-average decrease in magnitude up to 2 Wm^{-2} (both day and night). As with sensible heat flux, this decrease is a result of reduction to both $(1 - f_{\text{URB}})$ and G_{natural} . The decreased daytime natural surface skin temperature is nearly balanced by increased nocturnal temperature, reducing the local temperature gradient across the natural skin surface and, thus, G_{natural} . Increased grid-average f_{URB} at case 20 s favors weighting rooftop “ground” heat flux more heavily than road “ground” heat flux. This change favors decreased daytime ground heat flux ($\sim 2\text{--}3 \text{ Wm}^{-2}$) and slightly increased nighttime flux. The contribution to total ground heat flux, $G_{\text{urban}}f_{\text{URB}}$, shows a net increase in magnitude ($2\text{--}3 \text{ Wm}^{-2}$ during the afternoon, 1 Wm^{-2} at night), due to increased grid-average f_{URB} .

The RMSD of G_{total} (Fig. 10) over the urban core peaks at 32 Wm^{-2} around 17:00 UTC (13:00 LT), coincident with the time of its strongest magnitude (Fig. 8) and 24% of G_{total} . RMSD increases for case 10 s vs. progressively coarser cases, but with proportionally smaller increments than H_{total} or $I_{\text{V}}E_{\text{total}}$, approaching 30% of the total flux value for case 10 s vs. case 120 s.

4.4 Meteorological response

Within the urban canyon, the model estimated air temperature (T_c) scalar wind speed (u_c) and water vapor mixing ratio (q_c) are subject to variation in canyon geometry and heat flux. Comparing case 10 s and case 20 s, the increased ratio of R/R_W and slight daytime (nighttime) decrease (increase) of surface skin temperature along the canyon walls and road in case 20 s decrease grid-average T_c up to 0.2 K in the afternoon and increase up to 0.1 K overnight. The u_c quantity demonstrates a slight grid-average reduction (less than 0.1 m s^{-1}). This is anticipated due to reduced mean canyon space at higher urban intensity. The grid-average q_c shows little change. Local response in canyon meteorology is more substantial, vulnerable to change in the above-canopy wind speed and local canopy height. Versus case 20 s, the peak of T_c , u_c and q_c RMSD (Fig. 11) is approximately 0.3 K, 0.2 m s^{-1} and 0.2 g kg^{-1} , respectively. Normalized by the mean, u_c RMSD is greatest, though more precise diagnosis of street canyon flow requires more explicit resolution as in a computational fluid dynamics model. RMSD increases consistently for comparison of case 10 s vs. progressively coarser resolution test cases, though evening change in q_c shows some variability.

Above the canopy, there is also evidence of a response in the meteorology. Examining the sign of the Obukhov length scale (L : Obukhov, 1946; Monin and Obukhov, 1954), the static stability of the urban environment in these case studies shows a consistently unstable daytime surface layer after sunrise. A largely stable nighttime surface layer develops abruptly after sunset. Being a function of surface heat flux, the transition of L from daytime static instability to nighttime static stability is non-uniform and progresses inversely to the urban intensity. For Periods 1 and 2, (sunset $\sim 01:12$ UTC) most developed, open space type urban land cover surfaces become statically stable within 30 min of 23:00 UTC, low intensity urban $\sim 23:50$ UTC, medium intensity urban $\sim 00:30$ UTC and high intensity urban $\sim 01:30$ UTC. Low-level wind speed remains generally $\leq 3 \text{ m s}^{-1}$ across the grid. Model estimates reveal limited, sporadic areas of static instability overnight over the high intensity urban surfaces, otherwise vacillating

Sensitivity of mesoscale model urban boundary layer

D. D. Flagg and
P. A. Taylor

Title Page

Abstract

Introduction

Conclusions

References

Tables

Figures

⏪

⏩

◀

▶

Back

Close

Full Screen / Esc

Printer-friendly Version

Interactive Discussion



**Sensitivity of
mesoscale model
urban boundary layer**

D. D. Flagg and
P. A. Taylor

[Title Page](#)[Abstract](#)[Introduction](#)[Conclusions](#)[References](#)[Tables](#)[Figures](#)[⏪](#)[⏩](#)[◀](#)[▶](#)[Back](#)[Close](#)[Full Screen / Esc](#)[Printer-friendly Version](#)[Interactive Discussion](#)

between weak and strong static stability. Around the time of sunrise (~10:00 UTC), high intensity urban surface transition to static instability precedes the rest of the domain by about 30 min. The remaining urban surface types change between 10:40 and 11:00 UTC. Thus, local change in urban surface classification at some coarser representation may drastically alter the overlying model estimated static stability. This result is keenly pertinent to model applications sensitive to surface layer vertical mixing in the evenings and overnight. Assessment of the local dynamic stability by way of the bulk Richardson number (Ri_b : Richardson, 1920) clearly distinguishes the dynamically unstable daytime well-mixed ABL from the laminar flow above and also reveals some difference in the evening residual turbulence strength between days during Period 1. Changes in the surface representation from case 10 s to case 20 s provoke a patchwork of positive and negative change, mostly above 100 m a.g.l., but not enough to alter the flow classification.

Air temperature above the canopy responds to the change in T_s due to changing scale of surface representation. Predictably, re-classification of urban grid cells to water grid cells from case 10 s to 20 s dominates the latter, given a typical 15–20 K T_s difference in the afternoons. Wind direction subsequently influences the breadth of this effect. On the afternoon of 23 June, low-level easterly wind favors more substantial cold air advection resulting from increased water coverage in case 20 s, not found on 24 June (south-southeast winds) or 7 July (west-southwest winds). Later that day, after 21:00 UTC, a Lake Erie lake breeze front (LBF) penetrates the domain from the south-southwest. The exchange of medium intensity urban land grid cells for water grid cells along the eastern part of the Detroit River delays the advance of the LBF (Fig. 12). Some local LBF acceleration and deceleration are also evident across the grid when comparing case 10 s and 20 s. Coastline resolution to the east of Windsor also affects the placement of a thermal internal boundary layer on 24 June. As the synoptic-scale wind rotates from south to southeast during the day, the fetch incorporates a progressively longer period over the cooler Lake St. Clair surface prior to reaching eastern Detroit. Its expansion into the urban core region is accelerated in case 20 s vs. case

10 s, providing up to a 1.5 K difference locally in air temperature above the canopy ($T_a \sim 28$ m a.g.l.) between cases.

The RMSD of T_a peaks at 0.2 K in the early afternoon (Fig. 11) for case 10 s vs. 20 s, slightly less than RMSD of T_c . Comparing case 10 s to coarser resolutions, RMSD of air temperature shows only modest increases. Air temperature above the urban canopy (T_a) and higher in the ABL appears relatively insensitive to systematic change in the urban morphology except in local circumstances as described above.

The effect of changed surface representation has a dichotomous effect on TKE. Increased urbanization at case 20 s leads to a net increase in mean canopy height, promoting mechanical production of turbulence and resulting in a net gain in grid-average TKE near the surface. When the wind direction and strength favors advection of the daytime grid-average cooling influence of the increased water coverage in case 20 s, the grid-average cooler surface slightly weakens the strength of thermal plume updrafts and downdrafts, concurrently reducing TKE aloft within the boundary layer and thus slightly reducing grid-average model estimated h_{ABL} , parameterized according to TKE strength (Janjic, 2002).

Locally, as the buoyant production of TKE in the ABL varies according to change in surface thermal properties, and shifting wind direction varies TKE strength, so does the model-estimated h_{ABL} also vary. The RMSD of h_{ABL} reveals considerable variability during the daytime, peaking above 300 m in the early afternoon (Fig. 11). Comparing case 10 s vs. progressively coarser urban surface representations yields RMSD exceeding 400 m.

The variation of q with surface representation follows the change in h_{ABL} . Reduction of grid-average h_{ABL} at case 20 s reduces dry air entrainment from aloft and leads to a grid-average net increase of q (up to 0.1 g kg^{-1}) in the well-mixed layer during the afternoon. RMSD of q_a peaks at 0.2 g kg^{-1} in the afternoon vs. case 20 s, expanding up to 0.3 g kg^{-1} vs. case 120 s (Fig. 11).

With considerable variation in wind direction among Periods 1 and 2, the low-level (above-canopy) horizontal wind speed RMSD peaks between $0.5\text{--}0.7 \text{ m s}^{-1}$ during the

Sensitivity of mesoscale model urban boundary layer

D. D. Flagg and
P. A. Taylor

[Title Page](#)[Abstract](#)[Introduction](#)[Conclusions](#)[References](#)[Tables](#)[Figures](#)[⏪](#)[⏩](#)[◀](#)[▶](#)[Back](#)[Close](#)[Full Screen / Esc](#)[Printer-friendly Version](#)[Interactive Discussion](#)

afternoon for comparison of the neighborhood scale to coarser scales (Fig. 11). Corresponding wind direction RMSD peaks in the early afternoon during ABL growth, reaching 25° for comparison vs. case 20 s and up to 35° for case 120 s. This sensitivity is of particular interest to the Detroit-Windsor metropolitan area, where such deviation can affect the timing and extent of influence of on-shore flow or LBF penetration.

5 Conclusions

The sensitivity of model mesoscale meteorology to the scale of representation of the urban surface is explored over several summer periods in the Detroit-Windsor metropolitan area. The response includes both periodic change (as a function of daily heating) and stochastic change (as from change in the direction and magnitude of low-level flow in response to varying surface morphology). The “effective model” resolution of approximately 2.1 km in the finest grid inhibits explicit inter-case comparison of the fine scale structure that would be expected to develop in response to a changing surface morphology; the model dampens this part of the KE spectrum and with it the variance of sensitivity to the surface morphology. However, the surface energy budget and other near-surface meteorological quantities forced largely by the surface parameterizations can be expected to show demonstrable sensitivity to change in the surface representation.

In the surface energy budget, the natural surface component of the total latent heat flux $l_v E_{\text{natural}} (1 - f_{\text{URB}})$ and the urban surface component of the total sensible heat flux $(H_{\text{urban}} f_{\text{URB}})$ are most sensitive, showing a net grid-average daytime decrease and increase, respectively, of up to approximately 10 Wm^{-2} for change from a 10 to 20 arc-second resolution. The fractional urban coverage (f_{URB}) parameter, which determines the extent of vegetation cover, contributes substantially to this sensitivity. Current urban parameterizations yield particularly varied performance with regard to latent heat flux estimation, often a result of the treatment of vegetation (Grimmond et al., 2009). Local change in urban classification as a consequence of scale change yields RMSDs of 20–30% of the total heat flux.

Sensitivity of mesoscale model urban boundary layer

D. D. Flagg and
P. A. Taylor

Title Page

Abstract

Introduction

Conclusions

References

Tables

Figures

⏪

⏩

◀

▶

Back

Close

Full Screen / Esc

Printer-friendly Version

Interactive Discussion



Sensitivity of mesoscale model urban boundary layer

D. D. Flagg and
P. A. Taylor

Title Page

Abstract

Introduction

Conclusions

References

Tables

Figures

⏪

⏩

◀

▶

Back

Close

Full Screen / Esc

Printer-friendly Version

Interactive Discussion



In the absence of explicit resolution of flow in the urban boundary layer, there is potential benefit to the neighborhood scale of resolution of the urban environment with respect to boundary layer depth estimation and in the timing of lake-breeze frontal passages or thermal internal boundary layers. High urban intensity, as found in the urban core of major cities, is found to delay the onset of nocturnal static stability at the surface up to 2–3 h vs. non-urban surfaces. Increased urban intensity enhances mechanical production of turbulence kinetic energy just above the canopy, but has little influence of model estimated boundary layer depth. Scale of representation is also critical to cities with riparian or coastal interests, where temperature, turbulence kinetic energy and boundary layer depth are highly sensitive. Afternoon estimated boundary layer depth RMSD vs. the neighborhood scale exceeds 300 m, demonstrating significant sensitivity.

Modelers should be cognizant of the inherent error in state variable estimates evolving from a mesoscale urban surface parameterization. This study offers one attempt to quantify the nature and magnitude of sensitivity to scale and the potential error that arises with progressively coarser representations. Although the most acute response predictably corresponds to surface and low-level quantities, change in boundary layer depth and the timing of mesoscale circulations like lake-breeze fronts can yield broader impacts on real atmosphere simulations.

Appendix A

Symbols, acronyms and abbreviations

ABL	Atmospheric Boundary Layer
ACARS	Aircraft Communications Addressing and Reporting System
a.g.l.	Above Ground Level
AMDAR	Aircraft Meteorological Data Acquisition and Relay
AWIP	NCEP Eta/NAM 212 grid model analysis
BAQS-Met	Border Air Quality and Meteorology field campaign
C_H	bulk transfer coefficient for heat

Sensitivity of mesoscale model urban boundary layer

D. D. Flagg and
P. A. Taylor

Title Page

Abstract

Introduction

Conclusions

References

Tables

Figures

◀

▶

◀

▶

Back

Close

Full Screen / Esc

Printer-friendly Version

Interactive Discussion

CrpGrslnd	mixed cropland and grassland land surface type
CrpPast	mixed cropland and pasture land surface type
CrpWood	mixed cropland and woodland land surface type
CFD	Computational Fluid Dynamics
CRC	(NOAA) Coastal Resources Center
DecBfFor	deciduous broadleaf forest land surface type
DecNfFor	deciduous needleleaf Forest land surface type
DNS	Direct Numerical Simulation
DTW	Detroit-Windsor
E	kinematic moisture flux ($I_v E$ = latent heat flux)
f_{URB}	fractional urban coverage
g	gram
G	ground heat flux
G_{natural}	ground heat from the natural component of an urbanized grid cell
G_{total}	ground heat flux from the G_{urban} and G_{natural} components of a grid cell
G_{urban}	ground heat flux from the urban canopy
Grasslnd	grassland land surface type
GPS	Global Positioning System
h	normalized building height
h_{ABL}	atmospheric boundary layer depth
hPa	hecto-Pascal
H	sensible heat flux
H_{natural}	sensible heat from the natural component of an urbanized grid cell
H_{total}	sensible heat flux from the H_{urban} and H_{natural} components of a grid cell
H_{urban}	sensible heat flux from the urban canopy
Hz	Hertz
IrgCrpPst	irrigated cropland and pasture land surface type
JJA	June–July–August
kg	kilogram
km	kilometer
K	Kelvin
I_v	latent heat of vaporization
$I_v E$	latent heat flux
$I_v E_{\text{natural}}$	latent heat from the natural component of an urbanized grid cell
$I_v E_{\text{total}}$	latent heat flux from the $I_v E_{\text{urban}}$ and $I_v E_{\text{natural}}$ components of a grid cell

Sensitivity of mesoscale model urban boundary layer

D. D. Flagg and
P. A. Taylor

Title Page

Abstract

Introduction

Conclusions

References

Tables

Figures

⏪

⏩

◀

▶

Back

Close

Full Screen / Esc

Printer-friendly Version

Interactive Discussion

$i_v E_{\text{urban}}$	latent heat flux from the urban canopy
L	Obukhov length scale
LBF	Lake Breeze Front
LES	Large Eddy Simulation
LSM	Land Surface Model
m	meter
MHz	MegaHertz
MxlrgCpP	mixed dry and irrigated cropland and pasture land surface type
METAR	aviation routine weather report
MYJ	Mellor-Yamada-Janjic
MNR	Ministry of Natural Resources
NOAA	National Oceanic and Atmospheric Administration
NCEP	National Centers for Environmental Prediction
NLCD	National Land Cover Dataset
NRC	National Research Council
NWP	Numerical Weather Prediction
NWS	National Weather Service
ON	Ontario
p	pressure
Pa	Pascal
q	water vapor mixing ratio/component of turbulence kinetic energy
q_a	water vapor mixing ratio at the mid-point of the lowest model layer
q_c	urban canyon water vapor mixing ratio
R	normalized building width
Ri_b	bulk Richardson number
RANS	Reynolds Averaged Navier Stokes equations
RMSD	Root-Mean-Squared Deviation
RMSE	Room Mean Squared Error
R_w	normalized street width
s	second
T	temperature
T_a	air temperature at the mid-point of the lowest model layer
T_c	urban canyon air temperature
T_s	skin surface temperature
TKE	Turbulence Kinetic Energy

Sensitivity of mesoscale model urban boundary layer

D. D. Flagg and
P. A. Taylor

Title Page

Abstract

Introduction

Conclusions

References

Tables

Figures

⏪

⏩

◀

▶

Back

Close

Full Screen / Esc

Printer-friendly Version

Interactive Discussion

u_a	horizontal wind speed at the mid-point of the lowest model layer
u_c	urban canopy wind speed
u	(scalar) wind speed
u_θ	wind direction
UCM	Urban Canopy Model
UrbHint	developed, high intensity urban land surface type
UrbLint	developed, low intensity urban land surface type
UrbMint	developed, medium intensity urban land surface type
UrbOpss	developed, open space urban land surface type
USGS	United States Geological Survey
UTC	Universal Coordinated Time
VHF	Very High Frequency
W	Watt
WRF	Weather Research and Forecasting model
WRF-ARW	Advanced Research WRF
x	model-estimated variable
\hat{x}	model-estimated variable interpolated to observation space
y	observed variable
z_R	mean canopy height
β	moisture availability
Δx	grid cell width
$^\circ$	degree

Acknowledgements. This work was supported by the Ontario Ministry of the Environment, Transboundary Air Research Grant. This work was made possible by the facilities of the Shared Hierarchical Academic Research Computing Network (SHARCNET: www.sharcnet.ca) and Compute/Calcul Canada.

The authors thank Sunny Wong and Jinliang Liu (Ontario Ministry of the Environment) for access to Ministry of Natural Resources land surface data, Ms. Katherine Hayden (Environment Canada) for air pressure measurements from Twin Otter flights and Ms. Shama Sharma (York University) for Harrow VHF wind profiler data.

References

- Allwine, K. J., Leach, M. J., Stockham, L. W., Shinn, J. S., Hosker, R. P., Bowers, J. F., and Pace, J. C.: Overview of Joint Urban 2003 – An Atmospheric Dispersion Study in Oklahoma City, Symposium on Planning, Nowcasting and Forecasting in the Urban Zone, Seattle, Washington, USA, 11–14 January 2004, (S. CD-ROM, J7.1), 2004.
- Ballish, B. and Kumar, V.: Systematic Differences in Aircraft and Radiosonde Temperatures, *B. Am. Meteor. Soc.*, 89, 1689–1707, 2008.
- Barlow, J. and Coceal, O.: A review of urban roughness sublayer turbulence, Met Office Meteorology Research and Development, Exeter, UK, 2009.
- Bornstein, R.: The 2-D URBMET urban boundary layer model, *J. Appl. Meteorol.*, 14, 1459–1477, 1975.
- Bougeault, P. and Lacarrère, P.: Parameterization of Orography-Induced Turbulence in a Mesobeta-Scale Model, *Mon. Weather Rev.*, 117, 1872–1890, 1989.
- Chen, F. and Dudhia, J.: Coupling an advanced land-surface/hydrology model with the Penn State/NCAR MM5 modeling system. Part I: Model description and implementation, *Mon. Weather Rev.*, 129, 569–585, 2001.
- Cheng, H. and Castro, I.: Near wall flow over urban-like roughness, *Bound.-Lay. Meteorol.*, 104, 229–259, 2002.
- Chou, M.-D. and Suarez, M.: An efficient thermal infrared radiation parameterization for use in general circulation models, NASA Tech. Memo., 104606, 1994.
- Delage, Y. and Taylor, P.: Numerical studies of heat island circulations, *Bound.-Lay. Meteorol.*, 1, 201–226, 1970.
- Garratt, J.: *The atmospheric boundary layer*, Cambridge University Press, Melbourne, 1992.
- Grimmond, C. and Oke, T.: Aerodynamic Properties of Urban Areas Derived from Analysis of Surface Form, *J. Appl. Meteorol.*, 38, 1262–1292, 1999.
- Grimmond, C. S. B., Blackett, M., Best, M., Baik, J. J., Belcher, S., Bohnenstengel, S., Calmet, I., Chen, F., Dandou, A., Fortuniak, K., Gouvea, M., Hamdi, R., Hendry, M., Kondo, H., Krayenhoff, S., Lee, S.-H., Loridan, T., Martilli, A., Masson, V., Miao, S., Oleson, K., Pigeon, G., Porson, A., Salamanca, F., Steeneveld, G.-J., Tombrou, M., Voogt, J., and Zhang, N.: The International Urban Energy Balance Comparison Project: Initial Results from Phase 2, Seventh International Conference on Urban Climate, Yokohama, Japan, , A11-6, 29 June–3 July, 2009.

Sensitivity of mesoscale model urban boundary layer

D. D. Flagg and
P. A. Taylor

Title Page

Abstract

Introduction

Conclusions

References

Tables

Figures



Back

Close

Full Screen / Esc

Printer-friendly Version

Interactive Discussion



Sensitivity of mesoscale model urban boundary layer

D. D. Flagg and
P. A. Taylor

Title Page

Abstract

Introduction

Conclusions

References

Tables

Figures

⏪

⏩

◀

▶

Back

Close

Full Screen / Esc

Printer-friendly Version

Interactive Discussion



Gutiérrez, E. J., Gonzalez, J. E., Bornstein, R. D., Arend, M., Moshary, F., and Martilli, A.: Numerical Simulations of Sea Breeze Circulations and Urban Heat Islands in NYC with a High Resolution Urban-Mesoscaled Model (uWRF), Ninth Symposium on the Urban Environment, Keystone, Colorado, USA, 9.2, 2–6 August, 2010.

5 Hocking, A. and Hocking, W.: Turbulence anisotropy determined by wind profiler radar and its correlation with rain events in Montreal, Canada, *J. Atmos. Ocean. Tech.*, 24, 40–51, 2007.

Hong, S.-Y., Dudhia, J., and Chen, S.-H.: A Revised Approach to Ice Microphysical Processes for the Bulk Parameterization of Clouds and Precipitation, *Mon. Weather Rev.*, 132, 103–120, 2004.

10 Janjic, Z.: Nonsingular Implementation of the Mellor-Yamada Level 2.5 Scheme in the NCEP Meso model, NCEP Office Note No. 437, National Centers for Environmental Prediction, Camp Springs, Maryland, USA, 61 pp., 2002.

Kain, J.: The Kain-Fritsch convective parameterization: An update, *J. Appl. Meteorol.*, 43, 170–181, 2004.

15 Kain, J. and Fritsch, M.: Convective parameterization for mesoscale models: The Kain-Fritsch scheme, in: *The representation of cumulus convection in numerical models*, Meteor. Monogr. No. 24, American Meteorological Society, Boston, Massachusetts, USA, 165–170, 1993.

Kim, J. and Baik, J.: A numerical study of thermal effects on flow and pollutant dispersion in urban street canyons, *J. Appl. Meteorol.*, 38, 1249–1261, 1999.

20 Klein, P., Leidl, B., and Schatzmann, M.: Driving physical mechanisms of flow and dispersion in urban canopies, *Int. J. Climatol.*, 27, 1887–1907, 2007.

Kusaka, H. and Kimura, F.: Coupling a Single-Layer Urban Canopy Model with a Simple Atmospheric Model: Impact on Urban Heat Island Simulation for an Idealized Case, *J. Meteorol. Soc. Jpn.*, 82, 67–80, 2004.

25 Kusaka, H., Kondo, H., Kikegawa, Y., and Kimura, F.: A Simple Single-Layer Urban Canopy Model for Atmospheric Models: Comparison with Multi-Layer and Slab Models, *Bound.-Lay. Meteorol.*, 101, 329–358, 2001.

Lee, S.-H. and Park, S.-U.: A Vegetated Urban Canopy Model for Meteorological and Environmental Modeling, *Bound.-Lay. Meteorol.*, 126, 73–102, 2008.

30 Leonardi, S., Orlandi, P. S., Djenidi, L., and Antonia, R.: Direct numerical simulations of turbulent channel flow with transverse square bars on one wall, *J. Fluid Mech.*, 491, 229–238, 2003.

Macdonald, R.: Modelling the mean velocity profile in the urban canopy layer, *Bound.-Lay.*

Sensitivity of mesoscale model urban boundary layer

D. D. Flagg and
P. A. Taylor

Title Page

Abstract

Introduction

Conclusions

References

Tables

Figures

⏪

⏩

◀

▶

Back

Close

Full Screen / Esc

Printer-friendly Version

Interactive Discussion



Meteorol., 97, 25–45, 2000.

Mamrosh, R., Baker, R., and Jirikowic, T.: A Comparison of ACARS WVSS and NWS Radiosonde Temperature and Moisture Data, Sixth Symposium on Integrated Observing Systems, Orlando, Florida, USA, 6.14, 12–17 January 2002, 2002.

5 Martilli, A.: Numerical study of urban impact on boundary layer structure: Sensitivity to Wind Speed, Urban Morphology and Rural Soil Moisture, *J. Appl. Meteorol.*, 41, 1247–1266, 2002.

Martilli, A., Clappier, A., and Rotach, M.: An urban surface exchange parameterisation for mesoscale models, *Bound.-Lay. Meteorol.*, 104, 261–304, 2002.

Masson, V.: A physically-based scheme for the urban energy budget in atmospheric models, *Bound.-Lay. Meteorol.*, 94, 357–397, 2000.

10 Miao, S., Chen, F., LeMone, M. A., Tewari, M., Li, Q., and Wang, Y.: An Observational and Modeling Study of Characteristics of Urban Heat Island and Boundary Layer Structures in Beijing, *J. Appl. Meteorol. Clim.*, 48, 484–501, 2009.

Miao, S., Jiang, W., Wang, X., and Guo, W.: Impact assessment of urban meteorology and the atmospheric environment using urban sub-domain planning, *Bound.-Lay. Meteorol.*, 118, 133–150, 2006.

Miller, E., Wang, J., and Cole, H.: Correction for Dry Bias in Vaisala Radiosonde RH Data, in: Ninth ARM Science Team Meeting Proceedings, San Antonio, Texas, USA, 22–26 March, 1999.

20 Mills, G.: The Urban Canopy Layer Heat Island, IAUC Teaching Resources, available at: <http://www.urban-climate.org/> (last access: March 2010), 2004.

Mlawer, E., Taubman, S., Brown, P., Iacono, M., and Clough, S.: Radiative transfer for inhomogeneous atmosphere: RRMT, a validated correlated-k model for the longwave, *J. Geophys. Res.*, 102(D14), 16663–16682, 1997.

25 Monin, A. and Obukhov, A.: Basic laws of turbulent mixing in the atmosphere near the ground, *Tr. Akad. Nauk SSSR Geofiz. Inst.*, 24, 163–187, 1954.

Myrup, L.: A numerical model of the urban heat island, *J. Appl. Meteorol.*, 8, 908–918, 1969.

NOAA National Weather Service: Radiosonde Observations, available at: <http://www.ua.nws.noaa.gov/factsheet.htm> (access: March 2010), 2010.

30 Nunez, M. and Oke, T.: The energy balance of an urban canyon, *J. Appl. Meteorol.*, 16, 11–19, 1977.

Obukhov, A.: Turbulence in an atmosphere with a non-uniform temperature, *Trudy Inst. Theor. Geofiz. AN SSSR*, 1, 1946.

Sensitivity of mesoscale model urban boundary layer

D. D. Flagg and
P. A. Taylor

Title Page

Abstract

Introduction

Conclusions

References

Tables

Figures

⏪

⏩

◀

▶

Back

Close

Full Screen / Esc

Printer-friendly Version

Interactive Discussion



- Oke, T.: Canyon geometry and the nocturnal urban heat island: Comparison of scale model and field observations, *Int. J. Climatol.*, 1, 237–254, 1981.
- Oke, T.: The energetic basis of the urban heat island, *Q. J. Roy. Meteor. Soc.*, 108, 1–24, 1982.
- Oke, T.: *Boundary Layer Climates*, Routledge, New York, 1987.
- Richardson, L.: The supply of energy from and to atmospheric eddies, *Proceedings of the Royal Society of London A*, 97, 354–373, 1920.
- Rotach, M.: On the influence of the urban roughness sublayer on turbulence and dispersion, *Atmos. Environ.*, 33, 4001–4008, 1999.
- Roth, M.: Review of atmospheric turbulence over cities, *Q. J. Roy. Meteor. Soc.*, 126, 941–990, 2000.
- Sailor, D. J.: *Anthropogenic Heat and Moisture Emissions in the Urban Environment*, Seventh International Conference on Urban Climate, Yokohama, Japan, S-3, 29 June–3 July, 2009.
- Salamanca, F., Martilli, A., and Yagüe, C.: A numerical study of the urban boundary layer over Madrid during the DESIREX (2008) campaign with WRF, Ninth Symposium on the Urban Environment and 19th Symposium on Boundary Layers and Turbulence, Keystone, Colorado, USA., J3C.2, 2–6 August, 2010.
- Skamarock, W. C.: Evaluating Mesoscale NWP Models Using Kinetic Energy Spectra, *Mon. Weather Rev.*, 132, 3019–3032, 2004.
- Skamarock, W. C., Klemp, J. B., Dudhia, J., Gill, D. O., Barker, D. M., Wang, W. and Powers, J. G.: A Description of the Advanced Research WRF Version 2, NCAR Tech. Note 468+STR, National Center for Atmospheric Research, Boulder, Colorado, USA, 88 pp., 2007.
- Smagorinsky, J.: General circulation experiments with the primitive equations. Part I: The basic experiment, *Mon. Weather Rev.*, 91, 99–164, 1963.
- Srinivasan, R. and Bastian, M.: Twin Otter Operations in Southern Ontario in Support of Project BAQS-MET - Border Air Quality Study Meteorological – 2007, LTR-FR-285, National Research Council Canada, Ottawa, Ontario, Canada, 26 pp., 2008.
- Statistics Canada: Demographics –City of Windsor, available at: <http://www.citywindsor.ca/002358.asp>(last access: April 2010), 2006.
- Turner, D., Lesht, B., Clough, S., Liljegren, J., Revercomb, H., and Tobin, D.: Dry Bias and Variability in Vaisala RS80-H Radiosondes: The ARM Experience, *J. Atmos. Ocean. Tech.*, 20, 117–132, 2003.

United States Census Bureau: Annual Estimates of the Population of Metropolitan and Micropolitan Statistical Areas: 1 April 2000 to 1 July 2009, <http://www.census.gov/popest/metro/files/2009/CBSA-EST2009-alldata.csv> (last access: April 2010), 2010.

Vukovich, F.: A study of the atmospheric response due to a diurnal heating function characteristic of an urban complex, *Mon. Weather Rev.*, 101, 467–474, 1973.

Walton, A., Cheng, A., and Yeung, W.: Large-eddy simulation of pollution dispersion in an urban street canyon – Part 1: Comparison with field data, *Atmos. Environ.*, 36, 3601–3613, 2002.

Walton, A. and Cheng, A.: Large-eddy simulation of pollution dispersion in an urban street canyon – Part I: Idealised canyon simulation, *Atmos. Environ.*, 36, 3615–3627, 2002.

ACPD

10, 25909–25958, 2010

Sensitivity of mesoscale model urban boundary layer

D. D. Flagg and
P. A. Taylor

Title Page

Abstract

Introduction

Conclusions

References

Tables

Figures

⏪

⏩

◀

▶

Back

Close

Full Screen / Esc

Printer-friendly Version

Interactive Discussion



Sensitivity of mesoscale model urban boundary layer

D. D. Flagg and
P. A. Taylor

Table 1. Values assigned to gridded urban parameters in the WRF urban canopy model according to surface type.

Urban Surface Type Classification	Bldg. Height (m)	Roughness Length, Disp. Height (m)	Norm. Bldg. [Road] Width	Norm. Bldg. Height	Drag Coeff.	Bldg. Volume Parm.	Urban Fraction
Open Space	7	0.7, 1.4	0.50 [0.50]	0.337	0.037	0.28	0.10
Low Intensity	7	0.7, 3	0.50 [0.50]	0.337	0.053	0.28	0.35
Medium Intensity	10	1.0, 6	0.63 [0.37]	0.242	0.083	0.40	0.65
High Intensity	16	1.6, 11	0.81 [0.19]	0.190	0.123	0.64	0.90

Title Page

Abstract Introduction

Conclusions References

Tables Figures

⏪ ⏩

◀ ▶

Back Close

Full Screen / Esc

Printer-friendly Version

Interactive Discussion



Sensitivity of mesoscale model urban boundary layer

D. D. Flagg and
P. A. Taylor

Title Page

Abstract

Introduction

Conclusions

References

Tables

Figures

◀

▶

◀

▶

Back

Close

Full Screen / Esc

Printer-friendly Version

Interactive Discussion

Table 2. RMSE (top) and mean bias (bottom) of model estimates for selected variables vs. verification datasets including aircraft data (T. O. = “Twin Otter”), radiosonde (KDTX) and a VHF wind profiler (Harrow Profiler).

RMSE	Temp. (K)	Water Vapor Mixing Ratio (g kg ⁻¹)	Horiz. Wind Speed (m s ⁻¹)	Horiz. Wind Direction (°)	Comparison Points
T.O. Flgt #12 (3–4 July)	2.71	2.58	2.48	105.46	30
T.O. Flgt #13 (6–7 July)	3.01	5.44	2.11	47.53	43
KDTX (00:00 UTC 4 July)	3.77	0.71	2.84	7.79	65
KDTX (12:00 UTC 7 July)	4.01	0.70	2.96	18.98	58
Harrow Profiler (7 July)	<i>n/a</i>	<i>n/a</i>	1.92	25.33	270
Bias	Temp. (K)	Water Vapor Mixing Ratio (g kg ⁻¹)	Horiz. Wind Speed (m s ⁻¹)	Horiz. Wind Direction (°)	Comparison Points
T.O. Flgt #12 (3–4 July)	-2.52	-2.55	1.91	100.70	30
T.O. Flgt #13 (6–7 July)	-2.83	-4.90	1.61	-6.05	43
KDTX (00:00 UTC 4 July)	2.43	-0.06	0.87	-3.05	65
KDTX (12:00 UTC 7 July)	2.14	0.38	1.40	-12.67	58
Harrow Profiler (7 July)	<i>n/a</i>	<i>n/a</i>	-0.36	3.02	270

Sensitivity of mesoscale model urban boundary layer

D. D. Flagg and
P. A. Taylor

Table 3. Measurements and model estimates for two missed landing maneuvers during Twin Otter Flight #13, 7 July 2007. Airport measurements (CYQG, KDET) are taken from METAR, with scalar quantities measured at 2 m a.g.l. and wind measured at 10 m a.g.l. The height of Twin Otter measurements is a 1-min average. Model estimates are interpolated to the averaged Twin otter measurement height.

	Missed Landing: 10:10 UTC			Missed Landing: 10:50 UTC		
	CYQG (10:00)	Twin Otter (10:10)	Model (10:10)	KDET (10:53)	Twin Otter (10:50)	Model (10:50)
Measurement Hgt (a.g.l.)	2, 10 m	8 m		2, 10 m	68 m	
Temperature (K)	292.2	295.6	290.3	291.5	297.2	291.1
Mixing ratio (g kg ⁻¹)	10.2	15.9	10.2	10.2	15.6	9.7
Horiz. wind speed (m s ⁻¹)	1.5	1.2	7.3	1.5	2.9	2.8
Wind direction (°)	290	333	287	290	315	286

[Title Page](#)
[Abstract](#)
[Introduction](#)
[Conclusions](#)
[References](#)
[Tables](#)
[Figures](#)
[⏪](#)
[⏩](#)
[◀](#)
[▶](#)
[Back](#)
[Close](#)
[Full Screen / Esc](#)
[Printer-friendly Version](#)
[Interactive Discussion](#)

Sensitivity of mesoscale model urban boundary layer

D. D. Flagg and
P. A. Taylor

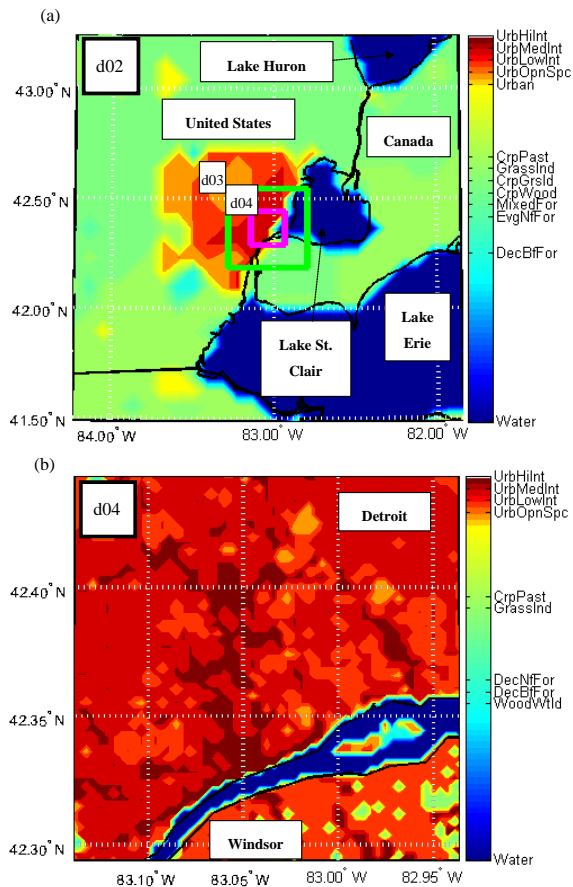


Fig. 1. Surface land cover type over the 2nd (a) and 4th (b) grids of the model domain over Detroit-Windsor (see Appendix A for abbreviations). Outlines of the 3rd grid (d03: green) and 4th grid (d04: magenta) appear in (a). The 1st grid (d01, not shown), is centered at 42.26° N, 93.10° W and extends across approximately 64° longitude and 29° latitude.

Title Page	
Abstract	Introduction
Conclusions	References
Tables	Figures
◀	▶
◀	▶
Back	Close
Full Screen / Esc	
Printer-friendly Version	
Interactive Discussion	

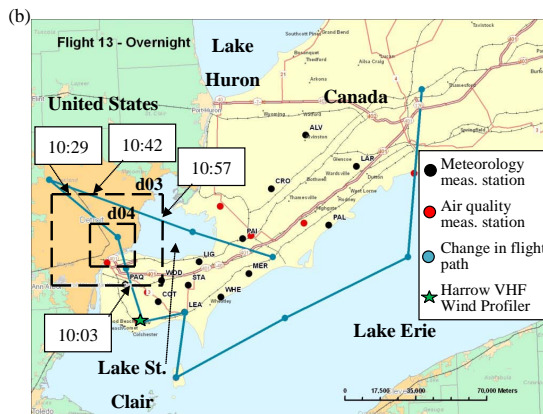
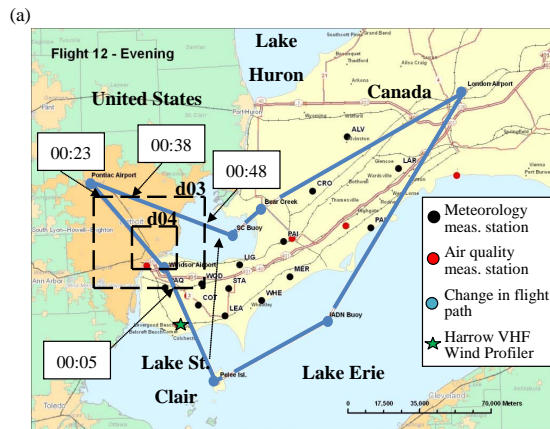


Fig. 2. The approximate flight paths of Flight #12 (a) and #13 (b) during BAQS-Met 2007, depicted by the blue line. The third (d03) and fourth (d04) model grid domains are outlined in dashed black lines with boxes indicating the approximate UTC time, 4 July 2007 (a), 7 July 2007 (b) upon entering and exiting the d03 domain. Adapted with permission from a figure by Julie Narayan, Environment Canada.

Sensitivity of mesoscale model urban boundary layer

D. D. Flagg and P. A. Taylor

Title Page

Abstract

Introduction

Conclusions

References

Tables

Figures

⏪

⏩

◀

▶

Back

Close

Full Screen / Esc

Printer-friendly Version

Interactive Discussion

Sensitivity of mesoscale model urban boundary layer

D. D. Flagg and P. A. Taylor

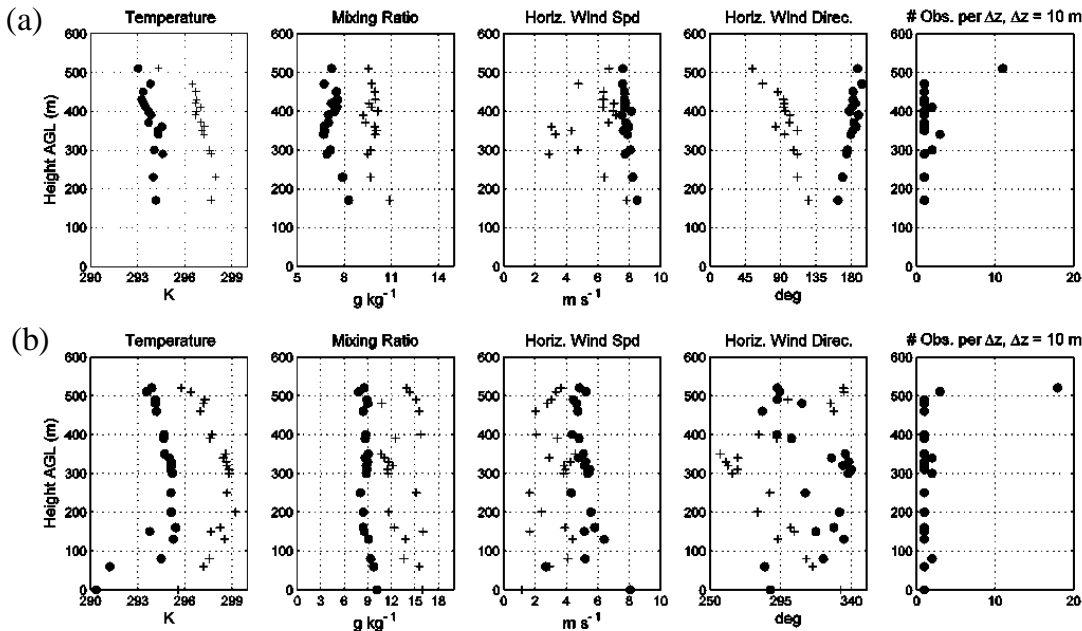


Fig. 3. Model verification vs. height using Twin Otter Flight #12, 3–4 July 2007 **(a)** and Flight #13, 6–7 July 2007 **(b)** measurements intercepting the third model grid. Variables depicted include: temperature, water vapor mixing ratio, scalar-average horizontal wind speed and horizontal wind direction. Model estimates are interpolated to observations and both are organized into 10 m bins. Each column shows the (bin-averaged) observed values (+) and model estimates (circles). The number of comparison points contributing to each bin is shown at the far right.

Title Page

Abstract	Introduction
Conclusions	References
Tables	Figures

⏪
⏩
◀
▶

Back	Close
------	-------

Full Screen / Esc

Printer-friendly Version

Interactive Discussion



Sensitivity of mesoscale model urban boundary layer

D. D. Flagg and
P. A. Taylor

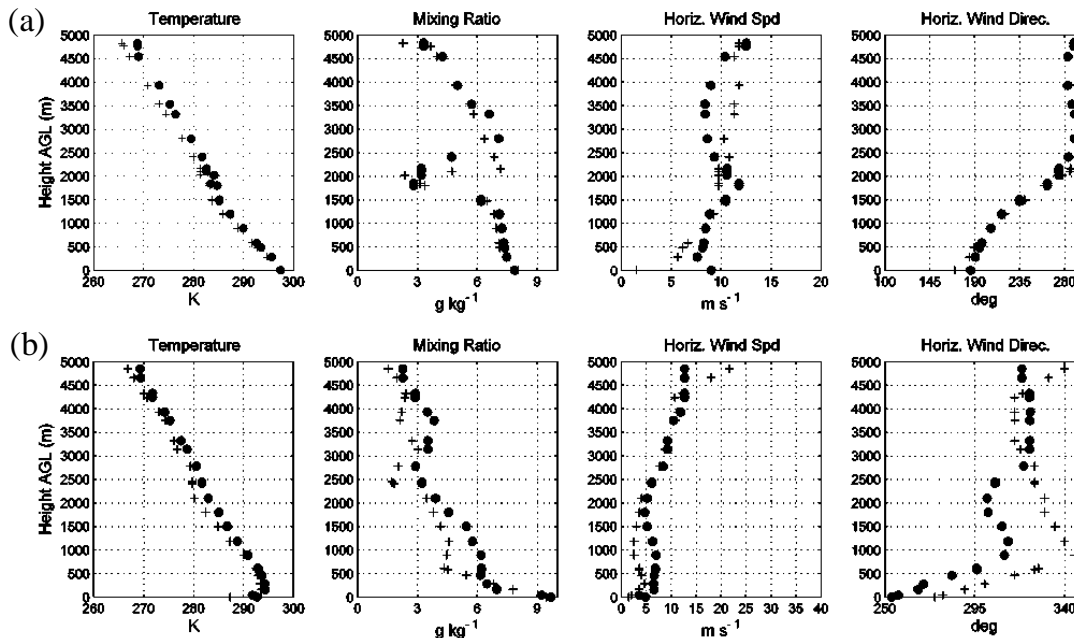


Fig. 4. Model verification vs. height using radiosonde measurements of temperature, water vapor mixing ratio, scalar average horizontal wind speed and horizontal wind direction in the lowest 5 km at KDTX (42°42' N 83°28' W) 00Z 4 July 2007 **(a)** and 12Z 07 July 2007 **(b)**. Model estimates are interpolated to observations and both are organized into 10 m bins. Each column shows the (bin-averaged) observed values (+) and model estimates (circles).

[Title Page](#)
[Abstract](#)
[Introduction](#)
[Conclusions](#)
[References](#)
[Tables](#)
[Figures](#)
[⏪](#)
[⏩](#)
[◀](#)
[▶](#)
[Back](#)
[Close](#)
[Full Screen / Esc](#)
[Printer-friendly Version](#)
[Interactive Discussion](#)

Sensitivity of mesoscale model urban boundary layer

D. D. Flagg and
P. A. Taylor

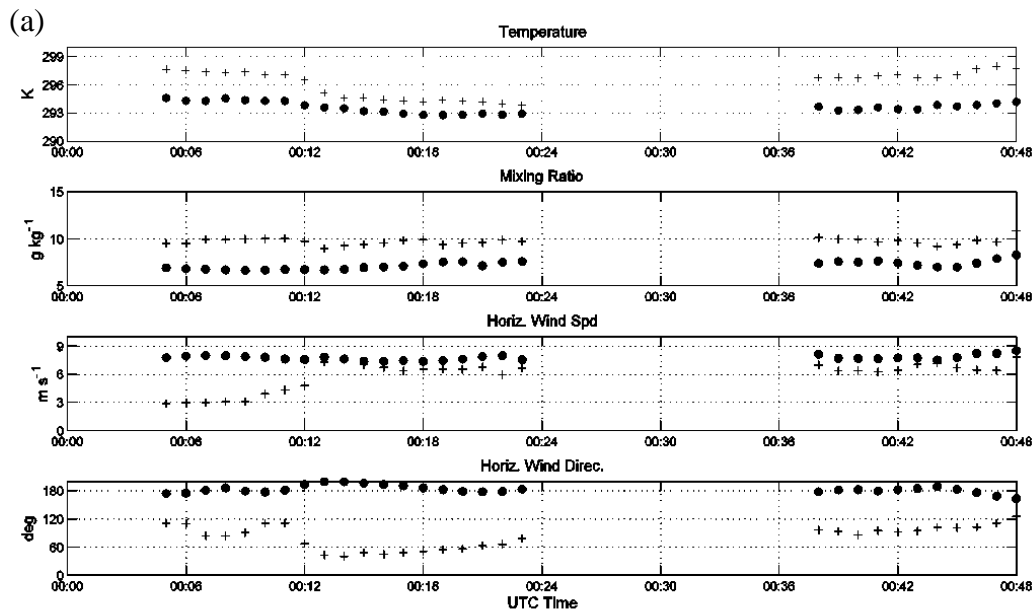


Fig. 5a. Model verification vs. time using Twin Otter Flight #12, 3–4 July 2007 (a) and Flight #13, 6–7 July 2007 (b) measurements intercepting the third model grid. Variables depicted include: temperature, water vapor mixing ratio, scalar-average horizontal wind speed, horizontal wind direction. Model estimates are interpolated to observations and both are organized into 1 min bins. Each row shows the (bin-averaged) observed values (+) and model estimates (circles).

[Title Page](#)[Abstract](#)[Introduction](#)[Conclusions](#)[References](#)[Tables](#)[Figures](#)[⏪](#)[⏩](#)[◀](#)[▶](#)[Back](#)[Close](#)[Full Screen / Esc](#)[Printer-friendly Version](#)[Interactive Discussion](#)

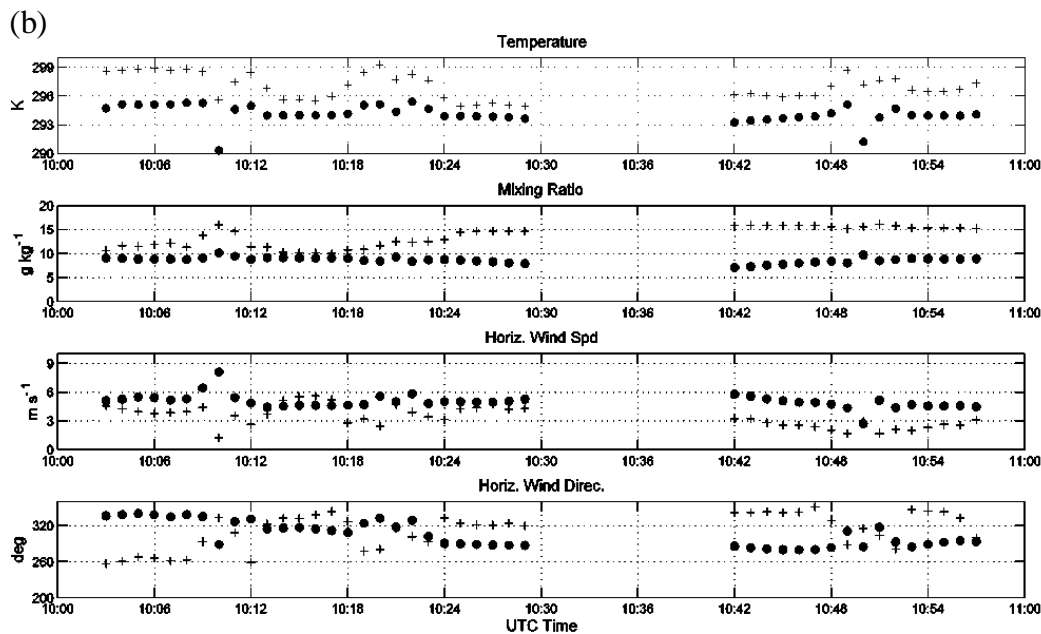
**Sensitivity of
mesoscale model
urban boundary layer**D. D. Flagg and
P. A. Taylor

Fig. 5b. Continued.

Title Page

Abstract

Introduction

Conclusions

References

Tables

Figures

◀

▶

◀

▶

Back

Close

Full Screen / Esc

Printer-friendly Version

Interactive Discussion

Sensitivity of mesoscale model urban boundary layer

D. D. Flagg and
P. A. Taylor

Title Page

Abstract

Introduction

Conclusions

References

Tables

Figures

◀

▶

◀

▶

Back

Close

Full Screen / Esc

Printer-friendly Version

Interactive Discussion

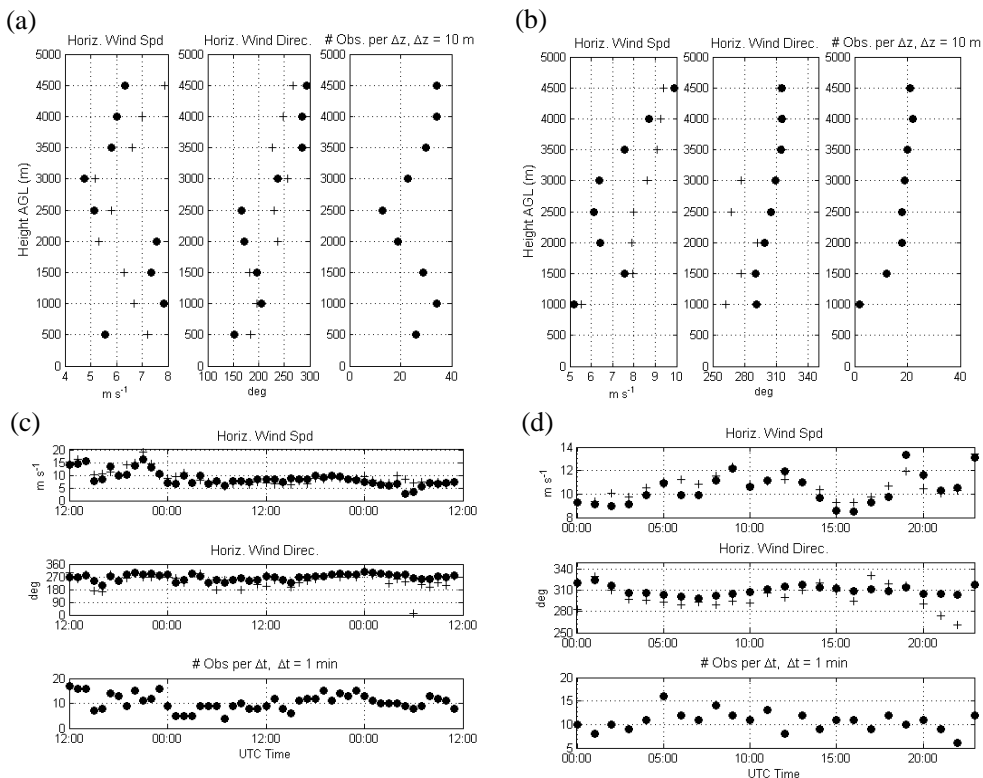


Fig. 6. Model verification vs. height (a, b) and time (c, d) using VHF wind profiler measurements of horizontal wind speed and direction. The wind profiler is located at Harrow, ON (42°42' N 83°28' W). Model estimates are interpolated to observations which are hourly mean values for the 500 m bin up to the height specified. Each row shows the (bin-averaged) observed values (+) and model estimates (circles). Data from Period 1 (a, c) and Period 2 (b, d) are shown. The number of observations contributing to each bin is illustrated in the third column (row) of the top (bottom) row graphs.

Sensitivity of mesoscale model urban boundary layer

D. D. Flagg and
P. A. Taylor

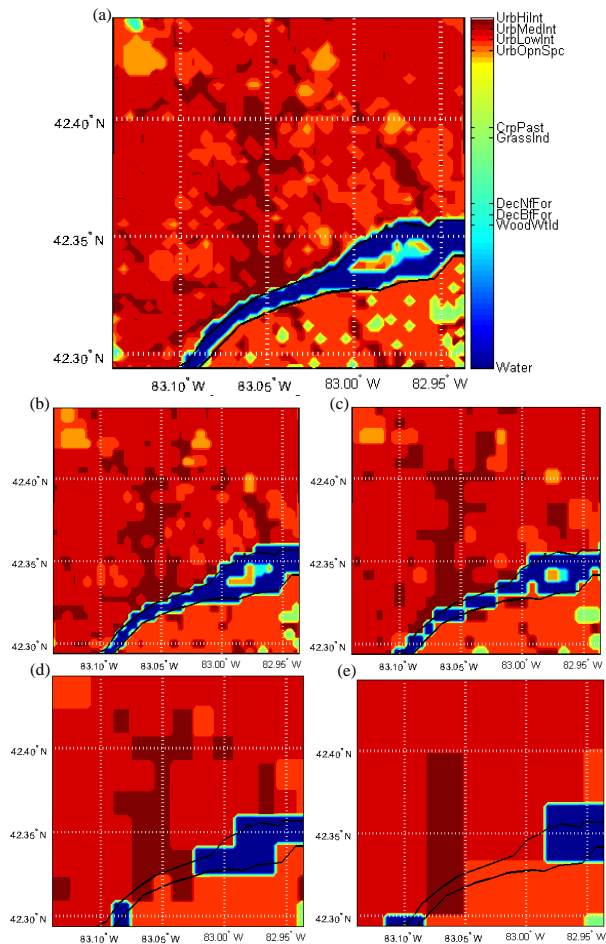


Fig. 7. Surface cover type over the fourth model grid of the Detroit-Windsor domain using 10 s (a), 20 s (b), 30 s (c), 60 s (d) and 120 s (e) surface cover resolution data. Color scheme in all subplots corresponds to that in (a). See Appendix A for translation of abbreviations in legend.

Sensitivity of mesoscale model urban boundary layer

D. D. Flagg and
P. A. Taylor

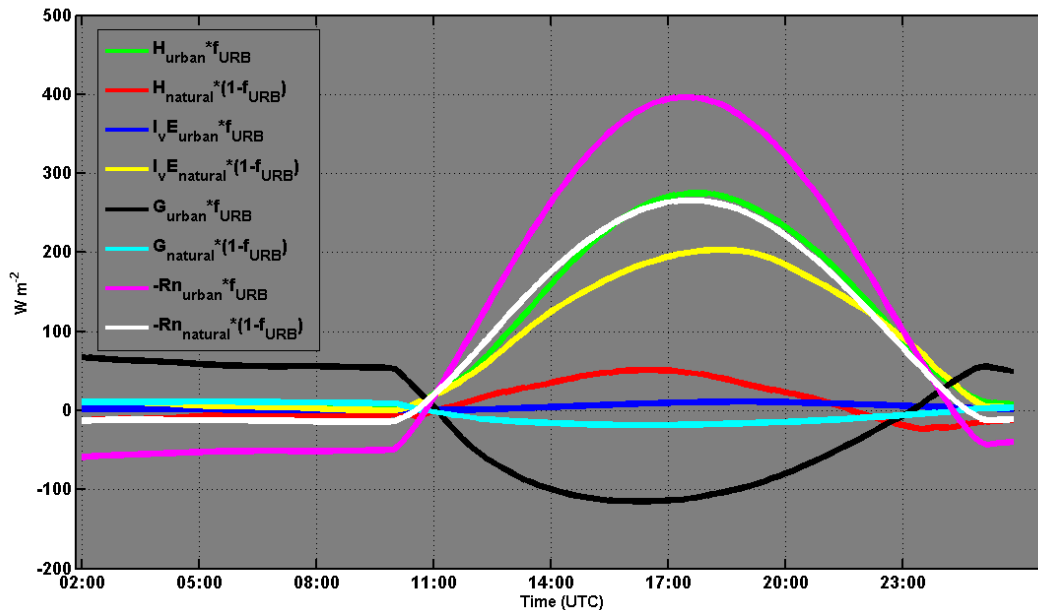


Fig. 8. Flux components of the average surface energy budget over the fourth model grid for case 10s. Fluxes are shown vs. time (UTC) for the period 02Z 24 June–01Z 25 June 2007 in units of W m^{-2} for the components: urban surface sensible heat (green), natural surface sensible heat (red), urban surface latent heat (blue), natural surface latent heat (yellow), urban surface ground heat (black), natural surface ground heat (cyan), (*negative*) urban surface net radiation (pink) and (*negative*) natural surface net radiation (white).

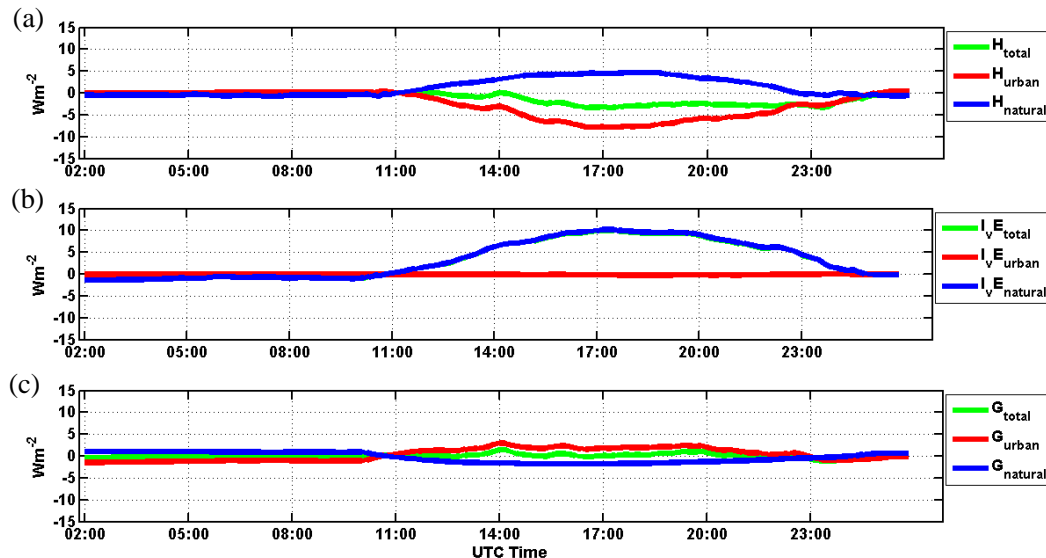
**Sensitivity of
mesoscale model
urban boundary layer**D. D. Flagg and
P. A. Taylor

Fig. 9. Change of flux (case 10 s–case 20 s) for sensible heat flux **(a)**, latent heat flux **(b)** and ground heat flux **(c)** including the total (green) urban (red) and natural surface (blue) contributions to each. Change shown is averaged over all grid cells in the fourth model grid of the domain, plotted vs. time (UTC) for the period 02Z 24 June–02Z 25 June 2007 in units of Wm^{-2} .

Title Page

Abstract

Introduction

Conclusions

References

Tables

Figures

◀

▶

◀

▶

Back

Close

Full Screen / Esc

Printer-friendly Version

Interactive Discussion

Sensitivity of mesoscale model urban boundary layer

D. D. Flagg and
P. A. Taylor

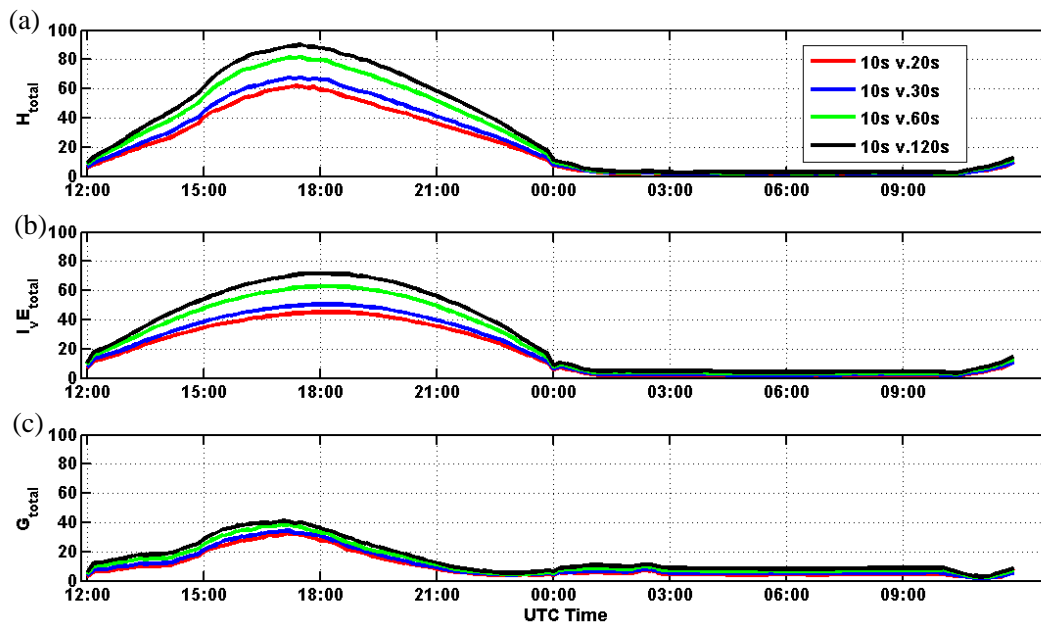


Fig. 10. RMSD of selected surface heat flux quantities over the fourth model grid for comparison of case 10 s and others of differing land cover resolution (in arc-seconds), averaged over all available data in Period 1 and Period 2. RMSD is shown vs. time of day (UTC time) in units of Wm^{-2} for total surface sensible heat flux **(a)**, total surface latent heat flux **(b)** and total ground heat flux **(c)**.

[Title Page](#)[Abstract](#)[Introduction](#)[Conclusions](#)[References](#)[Tables](#)[Figures](#)[◀](#)[▶](#)[◀](#)[▶](#)[Back](#)[Close](#)[Full Screen / Esc](#)[Printer-friendly Version](#)[Interactive Discussion](#)

Sensitivity of mesoscale model urban boundary layer

D. D. Flagg and
P. A. Taylor

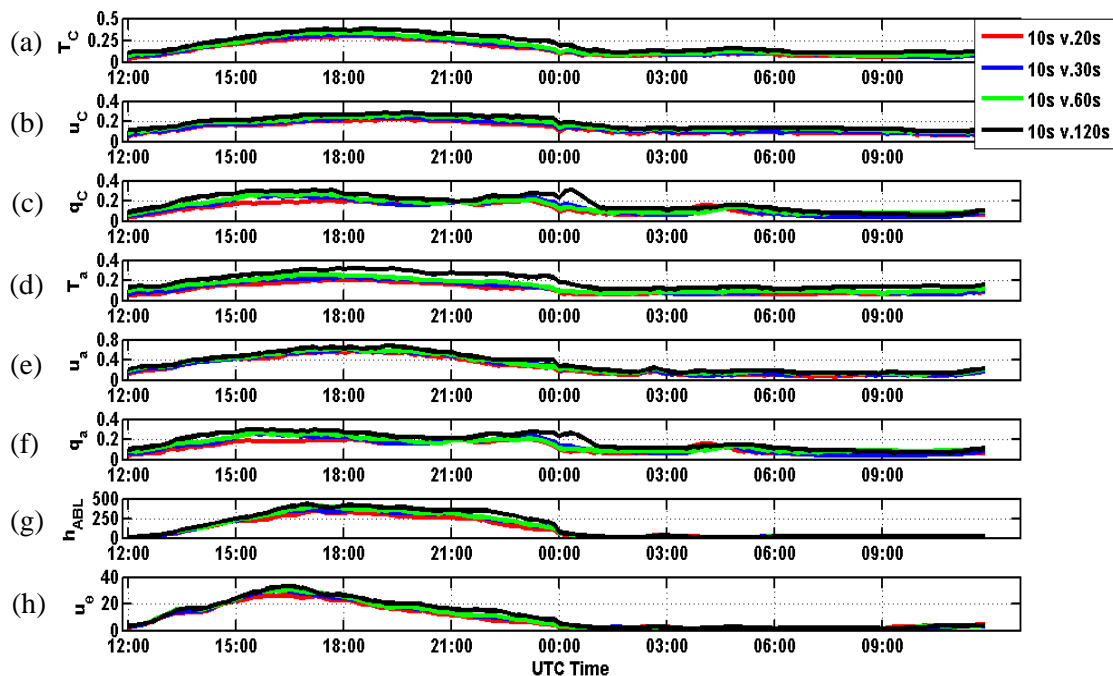


Fig. 11. RMSD of selected meteorological quantities over the fourth model grid for comparison of case 10s and others of differing land cover resolution (in arc-seconds), averaged over all available data in Period 1 and Period 2. RMSD is shown vs. time of day (UTC time) in units of K for **(a)** canyon temperature (T_c), m s^{-1} for **(b)** canyon wind speed (u_c), g kg^{-1} for **(c)** canyon water vapor mixing ratio (q_c), K for **(d)** lowest model layer (~ 28 m a.g.l.) temperature (T_a), m s^{-1} for **(e)** lowest model layer wind speed (u_a), g kg^{-1} for **(f)** lowest model layer water vapor mixing ratio (q_a), m for **(g)** boundary layer depth (h_{ABL}) and degrees for **(h)** lowest model layer wind direction (u_θ).

Sensitivity of mesoscale model urban boundary layer

D. D. Flagg and
P. A. Taylor

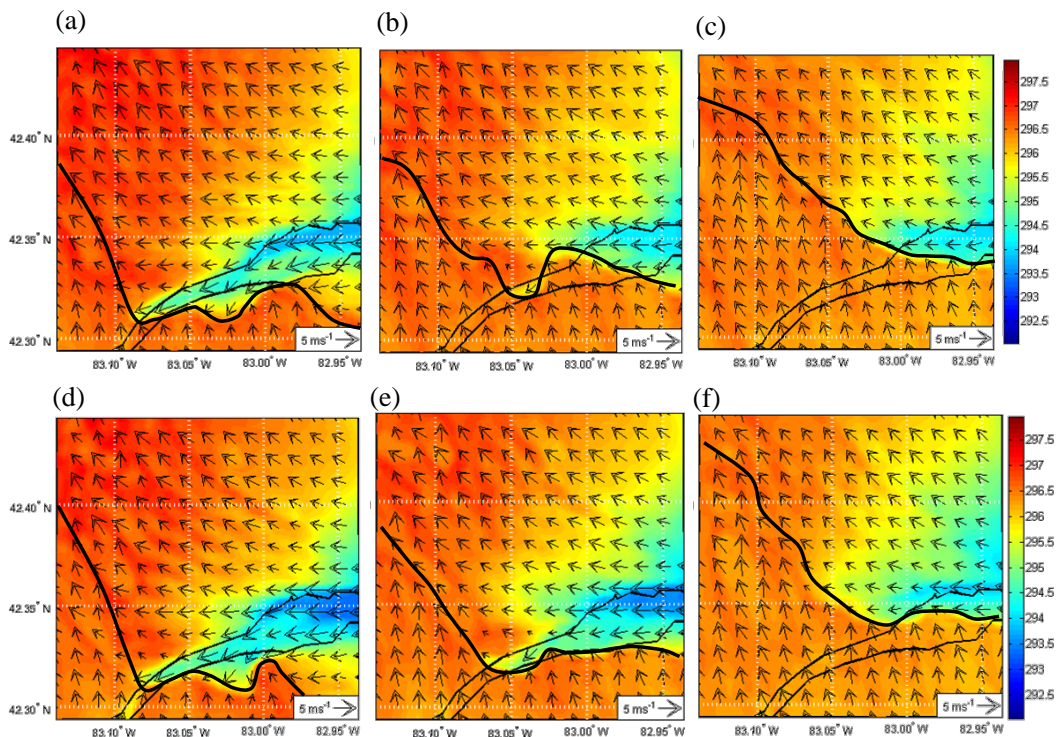


Fig. 12. Temperature (K), at the lowest model layer (~ 28 m a.g.l.) over the fourth model grid of the domain at 22:10 (**a, d**), 22:50 (**b, e**) 23:20 UTC (**c, f**) 23 June 2007 for case 10 s (**a to c**) and case 20 s (**d to f**). Horizontal wind speed for each case at this height is shown in vectors scaled by the key at the lower right. The estimated position of the lake breeze front is indicated by the thick black contour.

Title Page

Abstract

Introduction

Conclusions

References

Tables

Figures

◀

▶

◀

▶

Back

Close

Full Screen / Esc

Printer-friendly Version

Interactive Discussion